Marine Heatwaves in the Arabian Sea

Abhisek Chatterjee[1], Gouri Anil[2], Lakshmi R Shenoy[1,3]

[1]Indian National Centre for Ocean Information Services, Ministry of Earth Sciences, Hyderabad, India
[2]Cochin University of Science and Technology, Cochin, India
[3]Kerala University of Fisheries and Ocean Studies, Cochin, India
Correspondence to: Abhisek Chatterjee (abhisek.c@incois.gov.in)

Abstract. Marine heatwaves (MHWs) are prolonged warm sea condition events that can cause a destructive impact on marine ecosystems. The documentation of MHWs and assessment of their impacts is largely confined to a few regional seas or in global mean studies. The north Indian Ocean received almost no attention in this regard despite the fact that this ocean basin, particularly the Arabian Sea, is warming at the most rapid pace among the other tropical basins in recent decades. This study shows the characteristics of MHW events for the Arabian Sea during 1982-2019. Our analysis shows that the duration of MHWs exhibit a rapidly increasing trend of ~20 days/decade (1.5-2 count/decade) in the northern Arabian Sea and the southeastern Arabian Sea close to the west coast of India; which is more than 15 fold increase in the MHW days from the early 80s'. At the same time increase in MHWs frequency is ~1.5-2 events/decade, i.e. an increase of ~six fold, indicating more frequent and much longer heatwave events in the recent decade. Notably, since the beginning of the satellite record, the years 2010 and 2016 exhibit the maximum number of heatwave days when more than 75% of days of the pre-monsoon and summer-monsoon season experience heatwaves. The accelerated trend of the heatwave days is found to be driven by the rapid rise of the mean SST of the Arabian Sea in the recent decade. Moreover, longer heatwave days are also associated with the dominant climate modes. Among them, the Indian Ocean Basin mode via the decaying phase of the El-Niño is the most influencing mode contributing to more than 70-80% of observed heatwave days in this basin. Further analysis of the most prolonged observed heatwave during April-June 2010 indicates that surface heat flux associated with the weaker latent heat loss and the shallow mixed layer was the primary cause of this event. Further, we note that the pre-monsoon cyclonic storms in the Arabian Sea often contribute to the waning of such heatwaves in the basin.

1 Introduction

Sea surface temperature (SST) shows significant variability over a large spectrum of frequencies in space and time across the globe. However, there are times when extremes of such variability occur, causing severe stress to the local ecosystem and economies driven by such ecosystems. These warmer than normal extreme ocean conditions are referred to as Marine Heatwaves (MHWs) and are defined as prolonged anomalously warm ocean conditions exceeding a pre-defined threshold (Pearce et al., 2011; Hobday et al., 2016). These extreme warm SST conditions were first coined to describe the Ningaloo

Niño off the western coast of Australia during spring 2011 (Feng et al., 2013). These extreme warm events are shown to be responsible for widespread coral bleaching (Feng et al., 2013; Hughes et al., 2017), loss of Kelp forest off the coast of Australia and New Zealand (Wernberg et al., 2016; Thomsen et al., 2019), reduction in seagrass meadows (Arias et al., 2018) and widespread harmful algal blooms (Trainer et al., 2020). Further, these events have also been shown to impact economically important fishery industries in the northwest Atlantic (Mills et al., 2013), northeast Pacific (Cavole et al., 2016) and coastal Australia (Caputi et al., 2016). Owing to their devastating nature, MHWs and it's generating mechanisms received a lot of attention in the recent decade. Studies of major MHWs that appeared in various parts of the world over the last decade suggest that evolution and the forcing mechanisms of such events differ considerably from region to region and predominantly depend on the local air-sea coupling, atmospheric conditions, oceanic preconditions and remote climatic teleconnections (Holbrook et al., 2019; Oliver et al., 2021). For example, persistent large scale positive atmospheric pressure anomaly ridge caused unprecedented warm SST in the northeastern Pacific during 2013-2016 with anomalies exceeding more than 3^{o}C (Bond et al., 2015; Lorenzo and Mantua, 2016). A similar mechanism was at play during the summer of 2003 in the Mediterranean Sea (Olita et al., 2006) and in the Tasman Sea during the summer of 2017/18 off the coast of New Zeeland (Salinger et al., 2019). On the other hand, advection of warm water was found to be responsible for the widespread MHW along the western coast of Australia in 2011 (Feng et al., 2013), in the tropical ocean around Australia in 2015/2016 (Benthuysen et al., 2018), southeast of Australia in the Tasman Sea during 2015/16 (Oliver et al.,2017) and off the coast of California (Durazo et al., 2002). Climate variabilities also play a significant role in modulating MHWs in the tropical/extratropical oceans (Holbrook et al., 2019). Among them, El-Niño Southern Oscillation (ENSO) is shown to be the dominant climate mode that influences MHW occurrence and duration in the tropical Pacific (Holbrook et al., 2020). In the Indian Ocean, the positive phase of ENSO (Roxy et al., 2014; Chakravorty et al., 2014; Swapna et al., 2014), Indian Ocean Basin Mode (Klein et al., 1999; Du et al., 2009) and Indian Ocean Dipole mode (Saji et al., 1999; Chowdary and Gnanaseelan, 2007) favour warming of SST in large part of the basin. In the extratropics, in the interannual time scale, MHWs in the northeast Pacific is primarily associated with the positive phase of Pacific Decadal Oscillation (PDO). However, in the longer time scale, the Pacific Decadal Oscillation and North Pacific Gyre Oscillation (NGPO) contributes to the genesis of heatwaves (Lorenzo and Mantua, 2016). On the other hand, the North Atlantic oscillation (NAO) shows strong associations in the MHWs of the northwest Atlantic (Scannell et al., 2016).

Unfortunately, while the understanding of the genesis of MHWs across the globe advanced rapidly over the last decade, there is no study to document these events in the northern Indian Ocean. Moreover, over the last few decades, the Indian Ocean, particularly the Arabian Sea, has seen rapid warming at a rate much faster than the other tropical basins (Levitus et al., 2012). This warming not only shows a negative influence on the primary productivity of the Arabian Sea (Roxy et al., 2016) but also influences a shift in the phytoplankton community from diatoms to *Noctiluca scintillans* in the northern Arabian Sea (Goes et al., 2020), reduced rainfall in the Indian continent (Roxy et al., 2015) and increase flood in the Indian mainland (Ajaymohon and Suryachandra, 2008). Moreover, the frequency of cyclogenesis in the Arabian Sea has also increased over the last few

decades, primarily believed to be driven by this rapid rise in the SST (Murakami et al., 2020; Deshpande et al., 2021). However, the impact of persistent MHW on this enhanced cyclogenesis is still yet to be explored.

Further, the southeastern Arabian Sea and the northern Arabian Sea are also economically very important as they constitute one of the major fishing zones in the Arabian Sea. As per the recent report from Central Marine Fisheries Research Institute, India (CMFRI, 2007), total fish landing from the Indian exclusive economic zones (EEZ) is 2.49×10^6 tonnes during 2001-2005, and among them, 67% of the catch is from the eastern Arabian Sea (Shankar et al., 2018). Hence, like other parts of the global ocean, MHWs in this region are very likely significantly influencing the local marine ecosystem, the migration of species and the associated fishery-dependent economy. Therefore, documenting and understanding the genesis of MHWs in the Arabian Sea, particularly in the coastal oceans that possess significant economic importance, is necessary for better predicting these MHWs and assessing their impacts on this region. Hence, in this study, we document MHWs in the Arabian Sea with a particular emphasis on the coastal waters close to the west coast of India and try to decipher the possible physical mechanisms that influence the genesis of such heatwaves in this region. Next, Section 2 describes the data we use and the model configuration, experiments, and forcing. The observed trends in the MHWs are discussed in Section 3. The influence of the SST trend and the variabilities are given in Section 4. In Section 5, the impact of various climate modes is discussed. In Section 7, the role of different physical processes for the heatwaves during 2010 is presented. Finally, Section 7 summarises our main results and discuss the possible implications of this study.

2 Data and Methodology

2.1 Sea Surface Temperature and MHW Detection

To detect MHWs for the Arabian Sea, we have used daily NOAA OISST version 2 (Reynolds et al., 2007). The SST data are analysed for the period of 1982-2019 available on a $0.25^o \times 0.25^o$ grid. The MHW detection tool "*heatwaveR"* package (Schlegel and Smit, 2018) is used for MHW detection. This tool uses the MHW definition based on Hobday et al. (2016) and characterises MHW as an anomalous, warm, discrete event prolonged for more than five continuous days with SST more than a particular threshold. The threshold is defined from a fixed seasonal climatological baseline with warmer SST above the 90^{th} percentile of the daily variability. Two consecutive events within three days are considered as a single event. The climatological baseline is defined based on a fixed 30 year period 1982-2011. This seasonally varying threshold allows heatwaves events to occur at any season across the year. In order to understand the MHW characteristics, three heatwave metrics are evaluated here: MHW duration defined as the days between the start and end dates of an event, MHW intensity refers to maximum SST anomaly during an event, and MHW frequency calculated based on the number of events occur during a season or year.

2.2 Ocean Model

The model used in the present study is an ocean general circulation model based on Modular Ocean Model version 5 (MOM5; Griffies, 2012). The model configuration uses a hydrostatic and Boussinesq approximation. Model coordinates are discretised based on generalised orthogonal coordinates in horizontal and z*-coordinate in the vertical. The model domain extends from 30°E-120°E and 30°S-30°N with a uniform horizontal resolution of 0.25°×0.25° and 40 z* levels in the vertical. The model bathymetry is based on Sindhu et al. (2007), with a minimum depth set to 15 m. The horizontal mixing is based on Griffies & Hallberg (2000), and the vertical mixing scheme is based on Large et al. (1994). The horizontal friction is set to the lowest value to keep the model stable. The temperature and salinity fields are relaxed to climatological values (Chatterjee et al., 2012) with a time scale of 30 days within the 4° sponge layer at the open eastern and southern boundaries. Salinity at the surface is restored with a relaxation of 15 days. To realistically simulate the cross basin flow, the narrow Palk strait between India and Sri Lanka is closed in this model (Chatterjee et al., 2013, 2017).

2.2.1 Model experiments and forcing

The model is initially spin-up for 35 years from a state of rest, and then the interannual run was carried out for 1990-2018 using restart state of the ocean from the final year simulation of the climatological run. For forcing the model, surface momentum fluxes (zonal and meridional wind stress) and surface heat fluxes (shortwave radiation, longwave radiation, air temperature and 2 m specific humidity) are obtained from Tropflux data (Praveen et al., 2012, 2013). The precipitation and surface air pressure are obtained from the NCEP reanalysis product (Kalnay et al., 1996). The monthly climatological river discharge is based on Vörösmarty et al. (1996) and Papa et al. (2010) and is introduced over the top 15 m of the water column. The model is extensively validated for the north Indian Ocean in earlier studies (Chatterjee et al., 2013, 2019; Shankar et al., 2016, 2018; Vijith et al., 2016; Lakshmi et al., 2020). In order to analyse the model simulated anomaly for each variable, this 29-year interannual simulation is used to calculate a climatological field.

2.2.2 Mixed layer heat budget

In order to understand the dominant physical forcing in the genesis of MHWs, a volume-averaged mixed layer heat budget analysis has been carried out using the temperature and velocity fields taken from the model simulation. The mixed layer temperature tendency over the time-varying mixed layer and fixed region of area A is given by

$$\frac{\partial \overline{T}}{\partial t} = \underbrace{-\overline{\nabla_H T}}_{Adv_H} + \underbrace{\frac{1}{\rho C_P}\int_A \frac{Q}{h}\,dA}_{Q_v} \underbrace{-\overline{w\frac{\partial T}{\partial z}} - \frac{1}{Ah}\int_A \left(k_v \frac{\partial T}{\partial z}\right)_{-h}}_{Subsurface\ Process} \qquad (1)$$

Where T is the SST, t is time, and overbar represents volume averaged over the region A and within the time-varying mixed layer depth h. Adv_H is the horizontal advection of temperature, Q is the net surface heat flux corrected for shortwave penetration below the surface mixed layer, ρC_P is the specific heat capacity of seawater, w represents the vertical velocity and k_v is the

vertical eddy diffusivity. The vertical advection and diffusion together represent subsurface processes that influence mixed layer temperature.

3 Trends in the MHW

The north Indian ocean sees rapid warming during the pre-monsoon or spring intermonsoon (PRM; March-April-May) and the summer monsoon (SWM; June-July-August-September) seasons when the Inter-Tropical Convergence Zone moves to the northern hemisphere over the Indian landmasses. This is the time, the Indian Ocean warm pool covers a large part of the southern and eastern part of the Arabian Sea, and the SST reaches more close to 31^{o}C (Joseph, 1990; Vinayachandran and Shetye, 1991; Shenoi et al., 1999; Chatterjee et al., 2012). Interestingly, the underlying oceanic dynamics and the air-sea interactions differ significantly from PRM to SWM season (Schott and McCreary, 2001). During PRM, owing to the weaker winds and termination of winter convective mixing by early March, the mixed layer depth (MLD) becomes vary shallow (~20-30 m; Montégut et al., 2004), leading to a rapid increase in SST over a large part of the Arabian Sea (Vinayachandran and Shetye, 1991; Rao and Sivakumar, 1999; Vinayachandran et al., 2007). Further, the remotely forced propagating signals from the west coast of India also contribute to this warming in the southeastern Arabian Sea (SEAS) (Shenoi et al., 1999; Durand et al., 2004; Shankar et al., 2004). The intrusion of Bay of Bengal freshwater via advected by the coastal currents (Shenoi et al., 1999) and weaker latent heat loss resulting from low winds due to the orographic effect (Kurian and Vinayachandran, 2007) also helps in rapid SST warming over the SEAS during April-May. However, by late May, as the summer monsoon winds start to blow over the Arabian Sea, the SST cools rapidly along the western boundary of the Arabian Sea (Vinayachandran et al., 2021). However, the central and eastern Arabian Sea remains warm (> 28^{o}C) until July (Chatterjee et al., 2012). By August, SST drops below 28^{o}C over most parts of the Arabian Sea driven by cloud cover and strong wind-driven mixing (Phillips et al., 2021). It is likely that this mean SST rise during these two seasons possibly has a significant impact on the MHW genesis over this region and thus, studied separately.

Figure 1 shows the trend of various MHWs characteristics of the Arabian Sea (north of 5^{o}N). Annually, the number of MHW days increased significantly over the entire Arabian Sea (Figure 1a). The northern Arabian Sea and the southern Arabian Sea show the strongest annual increasing trend with a rate of ~3 days/year. A similar increasing trend is also noticeable in the Persian Gulf and the Gulf of Aden, two marginal seas connected to the Arabian Sea. The rest of the Arabian Sea, including the coastal water of India, shows an annual increase in the MHW days at a rate of 1.5-2 days/year. We find that PRM and SWM constitute most of the marine heatwave days observed annually across the years, with about 60% of heatwaves days occurring during these two seasons in the Arabain Sea. Notably, the trends of the heatwave days show marked spatial contrast between the two seasons (Figure 1d, g). During PRM season, the strongest trend is primarily limited to the northern Arabain Sea along the coast of Pakistan, the northwestern coast of India (coast of Gujarat and Maharastra), and the western boundary of the Arabian Sea along the coast of Arabia and Somalia. In comparison, the rest of the Arabian Sea does not show any notable

increase in heatwave days. On the other hand, during SWM, a significant increase in heatwave days is observed in the southeastern Arabian Sea, particularly all along the west coast of India. Additionally, the northern Arabian Sea continues to show a significant increasing trend similar to the PRM season but limited mainly along the coast of Iran, Pakistan and the northeast coast of India. The western Arabian Sea does not show any significant trend in heatwave days during this season.

The frequency of heatwaves also show a marginal annual increasing trend across the Arabian Sea, but the stronger trend of ~0.06-0.08 event/year is limited to the southern and northeastern Arabian Sea and all along the west coast of India (Figure 1b). During PRM and SWM season, the increasing trend of heatwave frequency is mostly collocated with the regions where an increasing trend of heatwave days is observed (Figure 1e, h). Therefore, while during the PRM season, an increasing trend in frequency is observed in the northern Arabian Sea region at a rate of ~0.1–0.15 event/year, the SWM season shows a similar trend along the west coast of India and across the southeastern Arabian Sea region. Note here that, annually, while the increase in the number of heatwaves over the four decades is only about 3-4 events, the heatwave days have increased by about 80-120 days. This indicates the duration of heatwaves turned much prolonged in the recent decade than that of the early 80s' and 90s'. On the other hand, heatwave intensity shows a meagre increase over most parts of the Arabian Sea. The most intense MHW intensity is experienced in the northern Arabian Sea, where an increasing rate of ~0.05^{o}C/year is observed during the PRM season.

Next, in order to understand the heatwave characteristics in detail, based on the observed trend of the various heatwave characteristics, we have selected two regions in the Arabian Sea for further analysis: the northern Arabian Sea (NAS; 60^{o}E-70^{o}E,18^{o}N-25^{o}N) and the southeastern Arabian Sea (SEAS; 65^{o}E-74^{o}E,7^{o}N-16^{o}N) (black boxes in Figure 1). Figure 2 shows the time series of percentage of heatwave days across each year annually and seasons-wise since 1982 for these two selected regions. In both regions, the number of heatwave days was comparatively low until the year 2000 except for the year 1986/87, 1992 and 1997/1998, coinciding with the initiation phase of the El-Niño and the positive phase of the Indian Ocean Basin Mode. Annually during this pre-2000 era, only ~5-10% of days experience heatwaves in these regions. After 2000, the number of heatwave days increased significantly, with an average of ~10-20% days experienced heatwaves in almost all years. Further, the rapid increase in heatwave days is observed from the year 2015 with at least 25-50% of days experienced heatwaves. During PRM season, the percentage of heatwave days is marginally higher in the NAS compared to the SEAS (Figure 2b, e). Moreover, as noted for annual, during PRM season, NAS shows a marked rise in heatwave days from the year 2015 with consistently more than 25-50% of days experienced heatwaves in this region. Nevertheless, during the entire satellite era, the year 2010 and 2016 stands out as both regions experienced heatwave for almost all days during this season. During SWM season, the characteristics of heatwave days remain similar as was observed in PRM (Figure 2c, f). The only exception is that since 2015, SEAS has experienced more heatwave days than the NAS. Notably, the summer of 2015, 2017 and 2019 exhibit at least 50% or more heatwave days in the SEAS.

Overall, there is a notable increasing trend of the heatwave days annually and for the PRM and SWM seasons. Notably, the number of heatwaves events annually also increased progressively over the years (Figure 3). Interestingly, the rapid increase in MHW days and frequency in the last decade coincides with the rapid mean SST warming of this region. This indicates that the anthropogenic warming of the mean SST is likely behind this increased heatwaves over this region. Further, most of the intense heatwave years also coincide with the El-Niño years, suggesting an important role of climate modes in modulating these extreme events in this region, which agrees with what is observed in other regional seas across the world ocean (Oliver et al., 2019).

4 Role of Indian Ocean Warming and SST Variability

The Indian Ocean has been warming rapidly over the last few decades. An estimate based on Enhanced Reconstructed Sea Surface Temperature (ERSSTv4) indicates that the tropical Indian Ocean is warming at a rate of 0.15ºC/decade during 1951-2015 (Roxy et al., 2020), this is particularly conspicuous during summer months (Roxy et al., 2014). SST trend calculated during the study period (1982-2019) for the Arabian Sea indicates that annual anomalous warming of ~1.5ºC in the recent decade is limited in the northern part of the Arabian Sea and ~0.75ºC in some parts of the southern Arabian Sea (Figure 4a). However, the season-wise SST trend shows pronounced spatial contrast between PRM and SWM seasons: while during PRM, NAS experiences anomalous warming of more than ~1.5ºC (Figure 4b), during SWM the warming of ~0.75-1ºC is located close to the west coast of India (Figure 4c). Notably, the regions with the strongest warming trend also experience an increasing trend of MHWs (see Figure 1), indicating that the warming of the mean SST contributes to the increasing trend of heatwave days in the Arabian Sea. This is in agreement with Oliver et al. (2019), who suggest that about 2/3rd of the global ocean experiences an increasing trend of heatwave days during the satellite period due to the rising mean temperature of the ocean. However, this observation is not very surprising partly due to the fact that we have used a fixed climatological baseline, and therefore, the rapid warming in the recent decade shifted the mean SST towards the heatwave threshold.

In order to understand the importance of the mean SST trend and the variability in the SST on the heatwave days over the Arabian Sea, the SST time series is decomposed as below:

$$T(t) = T^{tr}(t) + T^{var}(t), \quad (2)$$

here, $T(t)$ is the time series of SST, $T^{tr}(t)$ is the SST trend, and $T^{var}(t)$ is the SST anomaly after removing the trend. Figure 5 shows the time series of the percentage of heatwave days based on detrended SST time series (T^{var}). In this case, the duration of MHWs for each year and season is primarily driven by SST variability. The major contrast between heatwave days based on $T(t)$ and $T^{var}(t)$ (compare Figures 2 and 5) is that there is no secular trend in the heatwave days when calculated based on only SST variability. This supports that the increasing trend in the MHW days in the Arabian Sea is driven by the rising temperature of the mean SST and not the variability. It should be noted that the detection of MHWs is relative to a fixed baseline. If one were to use a moving baseline, warming SSTs would not necessarily lead to a trend in MHW days. Note also

that SST variability contributed most strongly during the PRM season of 2010 in the NAS region, with almost 50-75% of days of this season experiencing heatwaves due to SST variability (Figure 5b). The 2016 event was the second most event in this region, contributed strongly by the SST variability. In fact, as the next section shows, we find that El-Niño primarily drives these large number of heatwave days during PRM season via the positive phase of the Indian Ocean Basin mode. In contrast, in the SEAS, the SST variability contributed most for the year 2016 with almost 20-40% of the observed heatwave days. The other notable years are 1988, 1998 and 2003, when a considerable number of days experience heatwave in this region due to SST variability alone. On the other hand, during the SWM season, the contribution of SST variability is most notable for the years 1982, 1983, 1987, 1988, and 2010 in the NAS and the years 1983, 1987, 2003 and 2015 in the SEAS.

In order to compare the role of mean SST warming with the SST variability, Figure 6 shows that the time series of the ratio of the heatwave days owing to the SST trend and its variability by approximating Equation (2) as follows:

$$\frac{MHW(T^{tr})}{MHW(T^{var})} \approx \frac{MHW(T)}{MHW(T^{var})} - 1 \qquad (3)$$

assuming that MHW based on T^{tr} and T^{var} are independent of each other. This is a fairly good approximation as the seasonal climatology is prepared using a 30-year record and doesn't include the last decade when a rapid increase in SST is observed. Thus, it can provide useful insight of the role of the mean warming trend of SST on the MHW generation. It shows a very secular shift after the year 2000 in the driving force of the total annual heatwave days in the Arabian Sea. While, during the pre-2000 era, the natural variability of SST contributes most in driving the MHWs, post-2000, the warming trend of mean SST becomes the dominant factor. It also shows that the influence of mean SST warming increased very rapidly over the last two decades, which is expected to continue further under the unabated Indian Ocean warming. However, there are years when the ratio is much smaller when the climate mode driven variability contributes significantly to these extreme warm events as noted in Figure 5.

5 Role of Dominant Climate Modes

Indian Ocean dipole mode (IOD) and El-Niño Southern Oscillation (ENSO) are the two dominant climate modes that contribute to the SST variability of the tropical Indian Ocean in interannual timescale (Saji et al., 1999; Du et al., 2009). During the positive phase of the IOD, the western Indian Ocean shows anomalous warming, whereas the eastern Indian Ocean cools. In the negative phase, the sign of the SST anomaly reverses. Similarly, ENSO modulates the SST in the tropical Pacific, but the influence of ENSO can be felt in other basins as well through an atmospheric teleconnection via anomalous Walker circulation (Du et al., 2009; Roxy et al., 2014) and the inter-basin transport of water mass properties (Lee et al., 2015). During the positive phase of ENSO, i.e. during El-Niño, the western Indian Ocean shows warmer anomaly due to the weakening of the summer monsoon winds and increased shortwave radiation (Swapna et al., 2014). On the other hand, during La-Nina, most parts of the Indian Ocean experience cooler anomaly except the west coast of Australia where SST elevated due to heat

transport via Leeuwin current (Feng et al., 2013; Benthuysen et al., 2014). Note here that many IOD co-occurred with ENSO, and therefore, atmospheric teleconnections associated with ENSO are often considered to be one of the primary triggers of the IOD events (Allan et al., 2001). Nevertheless, there are many instances when extreme IOD appears in the absence of ENSO, suggesting the importance of regional processes within the Indian Ocean in the evolution of IOD (Ashok et al., 2003). However, considering the strong coupling between the ENSO and IOD mode, separating the effects of these modes on the Indian Ocean warming sometimes becomes challenging.

Additionally, associated with the direct impact of ENSO, the Indian Ocean warming mode (also referred to as Indian Ocean Basin mode; IOBM), which peaks during the decaying phase of the El-Niño and after the La-Nina, also contributes to the widespread warming of the tropical Indian Ocean (Xie et al., 2009). Notably, the initiation of IOBM mode is primarily caused by the ENSO induced suppressed atmospheric convection over the tropical Indian Ocean (Klein et al., 1999). However, it can act as a capacitor to influence atmospheric teleconnection till next summer in the decaying phase of the El-Niño (Xie et al., 2009). Hence, the warming of the Indian Ocean during the positive IOBM mode inherently contains the effect of previous El-Niño.

Similarly, North Atlantic Oscillation (NAO) has also been shown to play an important role in modulating SST of the Indian ocean in interannual to decadal time scale (Xie et al., 2021). Therefore, these climate modes can support the genesis or suppression of heatwaves depending upon their phases via modulating the thermocline depth and associated air-sea interactions of the basin (Holbrook et al., 2019, 2020; Oliver et al., 2021).

This section will look at the role of these climate modes, particularly IOD, ENSO, IOBM and NAO, on the genesis of MHWs in the Arabian Sea. As noted already in the previous section, the most number of heatwave days observed either during the initiation phase of El-Niño or during the decaying phase of the El-Niño (i.e. during the positive phase of the IOBM).
This indicates that the El-Niño and IOBM climate modes play a significant role in modulating heatwaves in this region. Figure 7a shows the correlation between MHW days derived from the detrended SST observation and the climate modes. ENSO shows the strongest correlation in the southcentral Arabian Sea with a correlation coefficient of ~0.5. The correlation decreases northward and, in fact, turns negative in the Persian Gulf region. This is in line with the correlation between Indian Ocean SST warming and the El-Niño mode (Roxy et al., 2014). The influence of IOD is most prominent in the western Arabian Sea in the vicinity of the western box of the IOD. Otherwise, the correlation is generally weak for the rest of the basin except close to the coast of Iran and Pakistan where a marginal increase in correlation is observed. However, note here that, unlike ENSO, the spatial and temporal length scale of IOD is much smaller. Thus, the correlation across the entire year maybe less, but it can still significantly influence a larger region during its peak phase. As expected, the IOBM, which represents the basin-wide warming mode of the tropical Indian Ocean, shows the strongest influence on the MHW days with a correlation coefficient of ~0.5 in most parts of the Arabian Sea. In this case also, like ENSO, the correlation decreases in the north. The influence of

NAO is the weakest among the other climate modes and is mostly limited to the SEAS region close to the southern part of the west coast of India during its negative phase.

As evident in the correlation map, the strong association of IOBM with the MHW days is also reflected in the large percentage of heatwaves days that co-occur with the positive phase of the IOBM (Figure 7b). Annually, about 60% and 75% of heatwave days co-occur with the positive IOBM in the NAS and SEAS, respectively. These co-existing numbers go much higher during the PRM season with more than 82% of heatwave days coincide with the positive IOBM phase in the SEAS region. The next most influencing climate mode is the positive phase of ENSO or El-Niño. This is more conspicuous during the PRM season as both the region experiences close to 50% co-existence between heatwave days and El-Niño. On the other hand, positive IOD also significantly co-exist with more than 40% of heatwave days during this season. During the SWM season, this association between IOBM and heatwaves decrease a bit with about 43% and 68% of heatwave days co-occur with the positive IOBM in the NAS and SEAS, respectively. The influence of El-Niño, on the other hand, show a marked difference between NAS and SEAS region. During summer, while in the SEAS, El-Niño co-occurs with ~50% heatwave days; in the NAS, both the phase (i.e. El-Niño and La-Nina) co-occur in ~20% heatwave days. This equal co-occurance of heatwave days in NAS indicates that there is no causal relationship between heatwave and ENSO in this region and therefore, possibly a mere coincidence. A similar relationship is observed for the IOD mode as well i.e. heatwaves during its positive and negative phase co-occur for an almost similar number of days and thus, hinted that IOD most likley don't cause heatwaves in the NAS during summer months. On the other hand, as seen in the correlation maps, the negative phase of NAO likely contributes to the genesis of MHWs in the SEAS with close to 20% of heatwave days coinciding with this mode during this season.

6 Dynamical mechanisms

The dynamical processes responsible for the genesis of MHWs across the global ocean vary significantly (Holbrook et al., 2019). Moreover, the processes may differ from one event to the other in a particular region. For example, different processes were involved in the consecutive observed MHW events in the South China Sea during 2016-2018 (Gao et al., 2020), in the northeast Pacific during 2014-15 (Di Larenzo et al., 2016) and 2019-20 (Chen et al., 2021) or along the southeastern Australian coast (Oliver et al., 2016; Li et al., 2020). The Arabian Sea also exhibits similar heterogeneity in the processes responsible for the genesis of MHWs across the seasons/years (more details are given in the discussion section). In this study, we analysed the heatwave event during the year 2010 as it was the longest observed event since the availability of the satellite observations and lasted for about 60-70 days (Figure 8 and 9). The initiation of the heatwave appears sometime in the last week of March in the northern and northeastern parts of the Arabian Sea when the SST is hovering around 27-29^{o}C, i.e. about 0.5^{o}C more than the threshold (Figure 10). By the third week of April, the heatwave event covers the entire northern part of the Arabian Sea. By May, with the northward movement of ITCZ, the entire Arabian Sea turns very warm with SST more than 31^{o}C. This intensifies the heatwave further to its peak and spreads along the western part of the Arabian Sea along the coast of Arabia

with an intensity of ~2°C. By the end of May, a low-level southwesterly surface wind (also known as Findlater Jet; Findlater, 1969) start to blow along the coast of Somalia, causing water to upwell along the coast (Schott and McCreary, 2001; Chatterjee et al., 2019; Vinayachandran et al., 2021). As the summer monsoon winds intensify, the upwelling signature extends all along the western boundary of the Arabian Sea. Thus, leading to a rapid decrease in SST in the western Arabian Sea cause the heatwaves to limit in the northeastern Arabian Sea close to the northwest coast of India. Finally, by mid-June, the heatwave event wanes off as the summer monsoon clouds set in across the western ghats of India.

The dominating processes involved in the generation of surface heatwaves in a particular region can be assessed through the analysis of heat sources and sinks in the upper mixed layer, which ultimately reflects in the variation of the SST. This approach was employed earlier for the understanding of the evolution of heatwaves during the 2011 Ningaloo Nino off Western Australia (Benthuysen et al., 2014), during 2012 warming off northeastern America (Chen et al., 2014) and in the East China Sea and the south Yellow Sea during the summer of 2016-2018 (Gao et al., 2020). Here, we have used a similar mixed layer heat budget formulation for the Arabian Sea (see Equation 1) to understand the dominant physical processes that likely favour this heatwave event's generation. The model could simulate the rapid rise of SST during this period, albeit with a cold bias of about 0.5°C (Figure 10). The spatial pattern of SST is also captured by the model quite well throughout the season (Figure 8 and 9), proving reasonable confidence to the mixed layer budget based on this model simulation. Note, however, that model is failed to simulate very short timescale SST variation (day-to-day), likely due to its resolution and coarser atmospheric flux used to force the model simulations.

Figure 11 shows the mixed layer heat budget at a point (63°E/19°N) located in the northcentral Arabian Sea and central to the NAS box. SST tendency starts to peak up by mid-March as the mixed layer soals to about 20 m over most of the Arabian Sea (Figure 12a), driven by weaker winds (Figure 13). The weaker winds further add to the weakening of the evaporative cooling resulting in an increase in the net surface heat flux (Q_v) (Figure 11) and therefore, rapid increase in SST (Figure 10). However, strong intraseasonal variability is evident primarily driven by the net surface heat flux (Q_v) owing to the intraseasonal variability in the surface winds. The anomalously shallow mixed layer during the pre-monsoon of 2010 (Figure 12b), owing to the weaker than normal winds driven by El-Niño atmospheric teleconnection, exaggerate the warming compared to the other years. The warming peaks in late April to early May as the Q_v continues to increase over the entire basin. As the summer monsoon winds peak up (Figure 13), thermocline deepens, and SST cools due to enhanced entrainment of cold subsurface water to the upper water column (Figure 11). Additionally, enhanced wind speed increases the latent heat loss (Figure 13) that further adds to the sharp decrease in Q_v and therefore, contributes to the further cooling of SST (Figure 10). In the subsequent days, SST recovers a bit with a weakly positive tendency before a sharp drop again on 1st June, 2010 driven by negative Q_v and strong entrainment cooling (Figure 11). This sharp drop in SST is linked to a severe cyclone *Phet.* The tropical cyclonic storm *Phet* was first developed on 31st May, 2010 in the central Arabian Sea around 1000 km west of Mumbai. It attended its peak wind speed of about 230 km/hr on 2nd June, 2010 and made landfall in eastern Oman on 3rd June, 2010 (See panel for

2nd June of Figure 8 for the cyclone track). The SST along this cyclone track decrease rapidly (more than 1^{o}C) and is contributed significantly to the weakening of the persisting heatwave in this region (Figure 9). After this cyclone, the SST recovers slightly but remains relatively cooler (Figure 10) due to the gradual decrease in shortwave flux and enhanced latent heat loss (Figure 13). It indicates that the cyclone *Phet* played a significant role in terminating the persisting heatwave in large part of the western Arabian Sea. Finally, the following intensification of summer monsoon winds and reduction in shortwave flux due to cloud cover reduced the SST further resulted in the waning of the heatwave event from the northern Arabian Sea.

7 Summary and discussion

In this study, we have investigated the trends and genesis of the MHWs in the Arabian Sea (north of 5^{o}N). Particularly we studied the three primary metrics of heatwaves: duration, frequency and intensity for the period of 1982-2019 and rallied primarily on the OISSTv2 SST observations. Further, we have also used an ocean model simulation based on Modular Ocean Model version 5 (MOM5) to conduct a mixed layer heat budget study for understanding the underlying forcing mechanism in the genesis of such heatwave events.

Like other regions of the world ocean, we find that the Arabian Sea also experiences a rapid increase in heatwave days. At the same time, heatwave frequency shows a marginal increase, suggesting that the heatwaves have now become prolonged and, in fact, sometimes persistent for an entire season in the recent decade. However, due to the weaker SST variability due to the proximity to the equatorial region, there is no significant increase in the heatwave intensity, a parameter often used to mark these events. Thus, this region remained unexplored in terms of MHWs in other global studies. The increasing trend of heatwave days is mainly evident post-2000 era and became conspicuous after 2015.

A detailed study for the pre-monsoon (or spring intermonsoon) and the summer monsoon indicates that the heatwave trend varies significantly across the seasons. During pre-monsoon, an increase in heatwave days at a rate of 15-20 days/decade is evident are primarily in the northern part of the Arabian Sea and along the coast of Arabia. However, during summer, the increasing trend at a similar rate is most evident all along the coast of India and over a large part of the southeastern Arabian Sea. Noticeably, across the last four decades, the years 2010 and 2016 show the longest heatwave days as the strong El Nino, on top of the mean warming trend, caused large and persistent warm SST across the Arabian Sea. An analysis of heatwave days based on detrended SST anomaly suggests that the enormous trend in the observed heatwave days are primarily linked to the rise in the mean SST of the Arabian Sea. The switch between the dominance of SST variability and the mean SST warming happened sometime around 2000. However, SST variability still contributes significantly for the years when climate variability is dominated by major climate modes and cause a significant source of SST warming in this basin. A detailed study of the association of heatwave days and these climate modes indicates that the Indian Ocean Basin mode (also referred to as Indian Ocean warming mode) via the decaying phase of the El-Niño influence very strongly influences the genesis of MHWs. In fact,

during pre-monsoon, when this Indian Ocean Basin Mode is most active, it co-exists in more than 70-80% of heatwave days. During the summer monsoon, its influence weakens over the entire Arabian Sea but remains significantly prominent in the southeastern Arabian Sea. However, co-existing days are reduced to merely 40% in the northern part, as evident in the correlation maps. The next most influencing climate modes are found to be El-Niño and positive IOD. These modes contribute to about 40-50% of heatwave days in the northern Arabian Sea during pre-monsoon. During the summer monsoon, the impact of these climate modes are relatively weaker but still contribute to more than 40% of heatwave days in the southeastern Arabian Sea. But, in the north, the influence of El-niño and IOD is almost negligible during this season.

The heatwave genesis and its forcing mechanisms vary considerably from year to year and within the Arabian Sea. A mixed layer heat budget shows a substantial heterogeneity in the forcing mechanisms of the genesis of MHWs in the Arabian Sea (Figure not shown). Considering that case studies designed for a particular heatwave event are necessary for such understanding, we analyse the possible forcing mechanisms for the longest (~70 days) and one of the intense (~2^{o}C) heatwaves over the study period observed during the pre-monsoon of the year 2010. Owing to the positive wind-evaporation-SST feedback during El-Nino of 2009-10 (Du et al., 2009), the 2010 springtime SST in the Arabian Sea show a strong positive tendency, leading to the formation of one of the strongest heatwaves in the recent decade (Figure 8). The heatwave starts to decay in the western Arabian Sea with the initiation of summer monsoon winds in the northern Indian Ocean. The upwelled water along the coast of Arabia limits the heatwave in the northeastern part of the Arabian Sea by late May. The decrease in net surface heat flux due to enhanced latent heat loss and reduced shortwave flux adds to the rapid cooling of SST during this period. Finally, the wind steering driven cooling associated with tropical cyclone *Phet* and subsequent intensification of summer monsoon weakens the heatwave further.

A similar process is also observed in the summer of 2020 when a severe cyclone *Nisagra*, which made landfall in Mumbai (a city located on the west coast of India), caused severe destruction by means of loss of life and property over a vast area, ended a one half month persistent heatwave of intensity more than 1^{o}C along the west coast of India (Figure 14 and 15). Interestingly, when we wrote this paper, another severe cyclone *Tauktae* hit the west coast of India and caused extensive damage to the property and life. This time, the SST was again more than 31^{o}C off the west coast of India. These similar events suggest that persistent extreme warm conditions like heatwaves may be linked to the increased cyclogenesis over the Arabian Sea in the recent decade. In fact, as the number of heatwave days increased significantly over the last two decades, the number of tropical cyclones also increased over the Arabian Sea (Figure 14), indicating a clear association between the heatwaves and the increased cyclogenesis in the Arabian Sea. In a recent study using a longer record, Deshpande et al. (2021) reported a 52% increase in the frequency of cyclonic storms over the Arabian Sea in recent decades. Further study is required to understand the dynamical links between heatwaves and associated atmospheric conditions to the observed enhanced cyclogenesis of this region.

This rapid increase in heatwave days in the northern and southeastern Arabian Sea is also likely to cause a severe impact on the physio-biogeochemical processes of this basin. One such possible impact is the recent increase in the harmful algal bloom in the Arabian Sea. Recent studies suggest that there is a manyfold increase in the harmful phytoplankton blooms in the northern Arabian Sea and along the west coast of India attributed primarily to the increased stratification, weaker winds and warming of the Arabian Sea (Padmakumar et al., 2012; Al Shehhi et al., 2014; Goes et al., 2020). Considering that the region of increased toxic blooms are collocated with the regions where the heatwave days are observed, the possibility that the relation between these heatwave events and the triggering of harmful blooms can not be neglected.

It is noteworthy that the heatwaves extremes are defined here using a fixed baseline of 1982-2011. Hence, considering that the recent decades have experienced a rapid rise in SST, the overall SST running mean is shifted more towards the heatwave threshold in the recent past. Therefore, if one were to use a moving baseline, warming SSTs would not necessarily lead to a trend in MHW days. The construct of MHW definition should take into account the ultimate impact we would like to address. The fixed baseline is possibly better suited when the impact on marine biology or atmospheric phenomena like cyclones are considered. Whereas the moving baseline may be a better choice if the effects of the warming trend are to be avoided. The implication of various such heatwave definitions is discussed in Oliver et al. (2021).

In summary, this study documented marine heatwaves and their various characteristics in the Arabian Sea. This is the first study where a detailed analysis of marine heatwave for the Arabian Sea, particularly for the coastal water of economic importance, is discussed. This study advocates further investigation of the impact of heatwave events on the coastal ecosystems and other oceanic properties of this tropical basin.

Author contribution

AC designed the study and wrote the paper, AC and GA performed the data analysis, LRS conducted the model experiments. All authors contributed to developing the research and contributed to the discussion.

Competing interests

The authors declare no competing interests.

Data availability

The daily OISST is obtained from https://coastwatch.pfeg.noaa.gov/erddap/. The daily north Atlantic oscillation index was provided by by NCEP Climate Prediction Centre (https://ftp.cpc.ncep.noaa.gov/cwlinks/). The best track data for cyclones are

obtained from the "Best Track Archive" of the Joint Typhoon Warning Centre. The model simulations will be made available upon request. The marine heatwave detection tool heatwaveR was taken from https://robwschlegel.github.io/heatwaveR/index.html.

Acknowledgement

The lead author thank the support provided by the Indian National Centre for Information Services (INCOIS), Ministry of Earth Sciences, to carry out this research. Funding for this work was provided from the "Deep Ocean Mission" programme of the Ministry of Earth Sciences, Government of India. The model simulations are carried out in the Ministry of Earth Science's central HPC facility, "MIHIR". A part of this work was based on the master's dissertation thesis of GA conducted at INCOIS. LRS was supported by the funding from INSPIRE DST fellowship. We acknowledge the critical comments from two anonymous reviewers; their comments have helped improve the paper significantly. Plotting and data analysis were carried out using R and Ferret software. This is INCOIS contribution number 0000.

References

Ajayamohon, R. S. and Suryachandra A. R.: Indian Ocean Dipole Modulates the Number of Extreme Rainfall Events over India in a Warming Environment, J. Met. Soc. Japan, 1, 245-252, 2008.

Al Shehhi, M. R., Gherboudj, I., Ghedira, H.: An overview of historical harmful algae blooms outbreaks in the Arabian Seas. Mar Pollut Bull., 86 (1-2), 314-324, 10.1016/j.marpolbul.2014.06.048, 2014.

Allan, Robert J. and Chambers, Don and Drosdowsky, Wasyl and Hendon, Harry and Latif, Mojib and Nicholls, Neville and Smith, Ian and Stone, Roger C. and Tourre, Yves: Is there an Indian Ocean dipole and is it independent of the El Niño-Southern Oscillation? CLIVAR Exchanges, 6 (3), 2001. pp. 18-22. ISSN 1026-0471

Arias- Ortiz, A., Serrano, O., Masqué, P., Lavery, P. S., Mueller, U., Kendrick, G. A., Rozaimi, M., Esteban, A., Fourqurean, J. W., Marbà, N., Mateo, M. A., Murray, K., Rule, M. J., and Duarte C. M.: A marine heatwave drives massive losses from the world's largest seagrass carbon stocks. *Nat. Clim. Change* **8**, 338–344, https://doi.org/10.1038/s41558-018-0096-y, 2018.

Ashok, K., Guan, Z., and Yamagata, T. (2003), Influence of the Indian Ocean Dipole on the Australian winter rainfall, Geophys. Res. Lett., 30, 2003. doi:10.1029/2003GL017926

Benthuysen, J., Feng, M. & Zhong, L.: Spatial patterns of warming off Western Australia during the 2011 Ningaloo Nino: Quantifying impacts of remote and local forcing. Cont. Shelf Res., 91, 232-246, 2014.

Benthuysen, J. A., Oliver, E. C. J., Feng, M., and Marshall, A. G. Extreme marine warming across tropical Australia during austral summer 2015–2016, J. Geophys. Res. 123, 1301–1326, 2018.

Bond, N. A., Cronin, M. F., Freeland, H., and Mantua, N.: Causes and impacts of the 2014 warm anomaly in the NE Pacific. Geophys. Res. Lett., 42**,** 3414–3420, 2015.

Caputi, N., Kangas, M., Denham, A., Feng, M., Pearce, A., Hetzel, Y., Arani, C.: Management adaptation of invertebrate fisheries to an extreme marine heatwave event at a global warming hot spot, Ecology and Evolution, 6(11), 3583–3593, https://doi.org/10.1002/ece3.2137, 2016.

Chatterjee, A., Shankar, D., Shenoi, S., Reddy, G., Michael, G., Ravichandran, M., Gopalkrishna, V. V., Rao, E. P. R., Bhaskar, T. V. S. U., and Sanjeevan, V. N. : A new atlas of temperature and salinity for the North Indian Ocean, Journal of Earth System Science, 121(3), 559–593, 2012.

Chatterjee, A., Shankar, D., McCreary, J., and Vinayachandran, P.: Yanai waves in the western equatorial Indian Ocean, Journal of Geophysical Research: Oceans, 118, 1556–1570, https://doi.org/0.1002/jgrc.20121, 2013.

Chatterjee, A., Shankar, D., McCreary, J., Vinayachandran, P., and Mukherjee, A.: Dynamics of Andaman Sea circulation and its role in connecting the equatorial Indian Ocean to the Bay of Bengal. Journal of Geophysical Research: Oceans, 122, 3200–3218. https://doi.org/10.1002/2016JC012300, 2017.

Chatterjee, A., Kumar, B. P., Prakash, S., and Singh, P.: Annihilation of the Somali upwelling system during summer monsoon, Scientific reports, 9(1), 7598. https://doi.org/10.1038/s41598-019-44099-1, 2019.

Chen, K., Gawarkiewicz, G. G., Lentz, S. J., Bane, J. M.:Diagnosing the warming of the northeastern U.S. coastal ocean in 2012: a linkage between the atmospheric jet stream variability and ocean response, J. Geophys. Res. Oceans, 119:218–27, 2014.

Chen, Z., Shi, J., Liu, Q., Chen, H., and Li, C.: A persistent and intense marine heatwave in the Northeast Pacific during 2019–2020. Geophysical Research Letters, 48, e2021GL093239, 2021. https://doi.org/10.1029/2021GL093239.

Chowdary, J. S. and Gnanaseelan, C.: Basin-wide warming of the Indian Ocean during El Niño and Indian Ocean dipole years, Int. J. of Clim., 27, 1421-1438, https://doi.org/10.1002/joc.1482, 2007, 2007.

Chakravorty, S., Chowdary, J. S., Gnanaseelan, C.: Epochal changes in the seasonal evolution of Tropical Indian Ocean warming associated with El Niño, Climate Dynamics, 42, 805-822, doi:10.1007/s00382-013-1666-3, 2014.

Cavole, L. M., Alyssa, M. D., Rachel, E. D., Ashlyn, G., Irina, K., Camille, M. L. S. P., May-Linn, P., Arturo, R.-V., Sarah, M. S., Nicole, K. Y., Michelle, E. Z., and Peter, J.S.:Biological Impacts of the 2013–2015 warm- water anomaly in the northeast Pacific: winners, losers, and the future, Oceanography, 29, 273–285, https://doi.org/10.5670/oceanog.2016.32, 2016.

CMFRI, 2007a. Marine fisheries profile India, http://www.cmfri.org.in/data-publications-/5/2007.

Deshpande, M., Singh, V.K., Ganadhi, M.K. et al. Changing status of tropical cyclones over the north Indian Ocean. Clim Dyn 57, 3545–3567 (2021). https://doi.org/10.1007/s00382-021-05880-z

Du, Y., Xie, S.-P., Huang, G. and Hu, K.: Role of air–sea interaction in the long persistence of El Niño–induced North Indian Ocean warming. *J. Climate*, **22**, 2023–2038, 2009.

Durazo, R., and Baumgartner, T. R.: Evolution of oceanographic conditions off Baja California. Prog. Oceanogr. 54, 7–31, 2002.

Durand F, Shetye SR, Vialard J, Shankar D, Shenoi SSC, Ethe C, Madec G.: Impact of temperature inversions on SST evolution in the South-Eastern Arabian Sea during the pre-summer monsoon season. Geophys Res Lett 31:L01305, 2004. doi:10.10.29-2003,GL018906

Feng, M., M. J. McPhaden, S.-P. Xie, and J. Hafner, 2013: La Niña forces unprecedented Leeuwin Current warming in 2011. Nature Sci. Repts., 3, 1277, doi 10.1038/srep01277.

Findlater, J.: Mean monthly air flow at low levels over the western indian ocean. Geophys. Mem. 115, 1969.

Gao, G., Marin, M., Feng, M., Yin, B., Yang, D., Feng, X., Ding, Y., Song, D.: Drivers of marine heatwaves in the East China Sea and the South Yellow Sea in three consecutive summers during 2016–2018, Journal of Geophysical Research:Oceans, 125, e2020JC016518, https://doi.org/10.1029/2020JC016518, 2020.

Goes, J.I., Tian, H., Gomes, H.d.R., Anderson, O. R., Khalid, A.-H., deRada, S., Luo, H., Lubna, A.-K., Adnan, A.-A., Martinson, D. G.: Ecosystem state change in the Arabian Sea fuelled by the recent loss of snow over the Himalayan-Tibetan Plateau region. Sci. Rep., 10, 7422, https://doi.org/10.1038/s41598-020-64360-2, 2020.

Griffies, S.M., and Hallberg, R.W.: Biharmonic friction with a Smagorinsky-like viscosity for use in large-scale eddy-permitting ocean models, MonthlyWeather Review, 128(8), 2935–2946, 2000.

Griffies, S. M.: Elements of the modular ocean model (MOM), GFDL Ocean Group Tech. Rep, 7, 620, 2012.

Hobday, A. J., Alexander, L. V., Perkins, S. E., Smale, D. A., Straub, S. C., Oliver, E. C. J., Benthuysen, J. A., Burrows, M. T., Donat, M. G., Feng, M., Holbrook, N. J., Moore, P. J., Scannell, H. A., Gupta, A. S., Wernberg, T.: A hierarchical approach to defining marine heatwaves, Prog. Oceanogr., 141:227–38, 2016.

Holbrook, N. J., Scannell, H. A., Gupta, A. S., Benthuysen, J. A., Feng, M., Oliver, E. C. J., Alexander, L. V., Burrows, M. T., Donat, M. G., Hobday, A. J., Moore, P. J., Perkins-Kirkpatrick, S. E., Smale, D. A., Straub, S. C., Wernberg, T.: A global assessment of marine heatwaves and their drivers. *Nat. Commun.* 10:2624, 2019.

Holbrook, N.J., Sen Gupta, A., Oliver, E.C.J., Hobday, A. J., Benthuysen, J. A, , Scannell, H. A., Smale, D. A., and Wernberg, T.: Keeping pace with marine heatwaves, Nat. Rev. Earth Environ., 1**,** 482–493, https://doi.org/10.1038/s43017-020-0068-4, 2020.

Hughes, T. P., Kerry, J. T. and Wilson, S. K.: Global warming and recurrent mass bleaching of corals. Nature, 543, 373–377, https://doi.org/10.1038/nature21707, 2017.

Joseph, P. V.: Warm pool over the Indian Ocean and monsoon onset, Trop. Ocean Atmos. Newsl., Winter, 53, 1 – 5, 1990.

Kalnay, E., Kanamitsu, M., Kistler, R., Collins, W., Deaven, D., Gandin, L., Iredell, M., Saha, S., White, G., Woollen, J., Zhu, Y., Chelliah, M., Ebisuzaki, W., Higgins, W., Janowiak, J., Mo, K. C., Ropelewski, C., Wang, J., Leetmaa, A., Reynolds, R., Jenne, R., and Joseph, D.: The NCEP/NCAR 40-year reanalysis project, Bull. Am. Meteorol. Soc., 77, 437–471, 1996.

Klein, S. A., Soden, B. J. and Lau, N.-C.: Remote sea surface temperature variations during ENSO: Evidence for a tropical atmospheric bridge. *J. Climate*, **12**, 917–932, 1999.

Kurian, J., and P. N. Vinayachandran: Mechanisms of formation of the Arabian Sea mini warm pool in a highresolution Ocean General Circulation Model, J. Geophys. Res., 112, C05009, 2007. doi:10.1029/2006JC003631.

Lakshmi, R. S., Chatterjee, A., Prakash, S., and Mathew, T.: Biophysical interactions in driving the summer monsoon chlorophyll bloom off the Somalia coast. Journal of Geophysical Research: Oceans, 125, https://doi.org/10.1029/2019JC015549, 2020.

Lee S.-K., Park, W., Baringer, M. O., Gordon, A. L., Huber, B., and Liu, Y.: Pacific origin of the abrupt increase in Indian Ocean heat content. Nature Geoscience, 8, 445-449, 2015.

Large, W. G., McWilliams, J. C., and Doney, S. C.: Oceanic vertical mixing: A review and a model with a nonlocal boundary layer parameterisation. Reviews of Geophysics, 32(4), 363–403, 1994.

Levitus, S., Antonov, J. I., Boyer, T. P., Baranova, O. K., Garcia, H. E., Locarnini, R. A., Mishonov, A. V., Reagan, J. R., Seidov, D., Yarosh, E. S. and Zweng, M. M.: World ocean heat content and thermosteric sea level change (0–2000 m), 1955–2010. Geophysical Research Letters 39(10). doi:10.1029/2012GL051106, 2012.

Li, Z., Holbrook, N. J., Zhang, X., Oliver, E. C. J., and Cougnon, E. A.: Remote Forcing of Tasman Sea Marine Heatwaves, Journal of Climate, 33(12), 5337-5354, 2020.

Lorenzo, E. D., Mantua, N.: Multi-year persistence of the 2014/15 North Pacific marine heatwave, Nature Cli. Change, 6, https://www.nature.com/articles/nclimate3082, 2016.

Mills, K. E., Andrew, J. P., Curtis, J. B., Yong, C., Fu-Sung, C., Daniel, S. H., Sigrid, L., Janet, A. N., Jenny, C. S., Andrew, C. T., Richard, A. W.:Fisheries management in a changing climate: lessons from the 2012 ocean heat wave in the Northwest Atlantic. *Oceanography* **26**, 191–195, 2013.

Montégut, de Boyer, C., Madec, G., Fischer, A. S., Lazar, A., and Iudicone, D. (2004), Mixed layer depth over the global ocean: An examination of profile data and a profile-based climatology, *J. Geophys. Res.*, **109**, C12003, doi:10.1029/2004JC002378.

Murakami, Hiroyuki, Delworth, T. L., Cooke, W. F., Zhao, M., Xiang, B. and Hsu, Pang-Chi: Detected climatic change in global distribution of tropical cyclones. *Proceedings of the National Academy of Sciences* **117**, 10706–10714, 2020.

Holbrook, N. J., Scannell, H. A., Gupta, A. S., Benthuysen, J. A., Feng, M., Oliver, E. C. J., Alexander, L. V., Burrows, M. T., Donat, M. G., Hobday, A. J., Moore, P. J., Perkins-Kirkpatrick, S. E., Smale, D. A., Straub, S. C., Wernberg, T.: A global assessment of marine heatwaves and their drivers. *Nat. Commun.* 10:2624, 2019.

Olita, A., Sorgente, R., Ribotti, A., Natale, S., and Gaberšek, S.: Effects of the 2003 European heatwave on the Central Mediterranean Sea surface layer: a numerical simulation. Ocean Sci. Discuss, 3, 85–125 (2006).

Oliver, E. C. J., Benthuysen, J. A., Bindoff, N. L., Hobday, A. J., Holbrook, N. J., Mundy, C. N., Perkins-Kirkpatrick, S. E.: The unprecedented 2015/16 Tasman Sea marine heatwave. *Nat. Commun.* 8:16101, 2017.

Oliver, E.: Mean warming not variability drives marine heatwave trends. Climate Dynamics 53 (3-4), pp. 1653-1659, 2019. doi: 10.1007/s00382-019-04707-2

Oliver, E. C. J., Benthuysen, J. A., Darmaraki, S., Donat, M. G., Hobday, A. J., Holbrook, N. J., Schlegel, R. W., Gupta, A. S.: Marine heatwaves, Ann. Rev. Mar. Sci., 13, 313-342, https://doi.org/10.1146/annurev-marine-032720-095144 , 2021.

Padmakumar, K. B., Menon, N. R., Sanjeevan, V. N.: Is Occurrence of Harmful Algal Blooms in the Exclusive Economic Zone of India on the Rise? Int. J. of Ocean., 2012, 1-7, https://doi.org/10.1155/2012/263946, 2012.

Papa, F., Durand, F., Rossow, W. B., Rahman, A., and Bala, S. K.: Satellite altimeter-derived monthly discharge of the Ganga-Brahmaputra River and its seasonal to interannual variations from 1993 to 2008, Journal of Geophysical Research, 115, C12013, https://doi.org/10.1029/2009JC006075, 2010.

Pearce, A. F., Lenanton, R., Jackson, G., Moore, J., Feng, M., Gaughan, D.: The "marine heat wave" off Western Australia during the summer of 2010/11, Tech. Rep. 222, West. Aust. Fish. Mar. Res. Lab., North Beach, Australia, 2011.

Phillips, H. E., Tandon, A. et al.: Progress in understanding of Indian Ocean circulation, variability, air–sea exchange, and impacts on biogeochemistry, Ocean Sci., 17, 1677-1751, 2021. https://doi.org/10.5194/os-17-1677-2021.

Praveen, K. B., Vialard, J., Lengaigne, M., Murty, V., and Mcphaden, M. J.: TropFlux: Air-sea fluxes for the global tropical oceans-description and evaluation. Climate Dynamics, 38(7-8), 1521–1543, 2012.

Praveen, K. B., Vialard, J., Lengaigne, M., Murty, V., Mcphaden, M. J., Cronin, M., Pinsard, F., Gopala, R. K.: TropFlux wind stresses over the tropical oceans: Evaluation and comparison with other products. Climate Dynamics, 40(7-8), 2049–2071, 2013.

Rao, R. R. and Sivakumar, R.: On the possible mechanisms of the evolution of a mini-warm pool during the pre-summer monsoon season and the genesis of onset vortex in the south-eastern Arabian Sea, Quart. J. Roy. Met. Soc., 125, 787-809, 1999.

Reynolds, R. W., Smith, T. M., Liu, C., Chelton, D. B., Casey, K. S., and Schlax, M. G.: Daily high-resolution-blended analyses for sea surface temperature, Journal of Climate, 20(22), 5473–5496, https://doi.org/10.1175/2007JCLI1824.1, 2007.

Roxy, M., Ritika, K., Terray, P. and Masson, S.: The curious case of Indian Ocean warming, *J. Climate*, 27, 22, 8501-8509, 2014.

Roxy, M., Ritika, K., Terray, P., Murtugudde, R., Ashok, K., Goswami, B. N.: Drying of Indian subcontinent by rapid Indian Ocean warming and a weakening land-sea thermal gradient. Nat. Commun., 6, https://doi.org/10.1038/ncomms8423, 2015.

Roxy, M. K., Modi, A., Murtugudde, R., Valsala, V., Panickal, S., Prasanna, K. S., Ravichandran, M., Vichi, M., and Lévy M.: A reduction in marine primary productivity driven by rapid warming over the tropical Indian Ocean, Geophys. Res. Lett., 43, 826–833, doi:10.1002/2015GL066979, 2016.

Roxy, M. K. , Gnanaseelan, C., Parekh, A., Chowdary, J. S., Singh, S., Modi, A., Kakatkar, R., Mohapatra, S., and Dhara, C.: Indian Ocean warming, In Assessment of Climate Change over the Indian Region, Krishnan, R., Sanjay, J., Gnanaseelan, C., Mujumdar, M., Kulkarni, A., Chakraborty, S., Eds., Springer, https://doi.org/10.1007/978-981-15-4327-2, 2020.

606 Saji, N. H., Goswami, B. N., Vinayachandran, P. N. and Yamagata, T.: A dipole mode in the tropical Indian
607 Ocean. *Nature*, **401**, 360–363. 1999.
608 Salinger MJ, Renwick J, Behrens E, Mullan AB, Diamond HJ, Sirguey, P., Smith, R. O., Trought, M. C. T., Alexander V, L.,
609 Cullen, N. J.: The unprecedented coupled ocean-atmosphere summer heatwave in the New Zealand region 2017/18: drivers,
610 mechanisms and impacts. Environ. Res. Lett., 14:044023, 2019.
611 Scannell, H. A., Pershing, A. J., Alexander, M. A., Thomas, A. C. and Mills, K. E.: Frequency of marine heatwaves in the
612 North Atlantic and North Pacific since 1950, Geophys. Res. Lett., 43, 2015GL067308, 2016.
613 Schott, F., and J. P. McCreary (2001), The monsoon circulation of the Indian Ocean, Prog. Oceanogr., 51, 1–123.
614 Schlegel, R. W. and Smit, A. J.: heatwaveR: A central algorithm for the detection of heatwaves and cold-spells. Journal of
615 Open Source Software, 3(27), 821, https://doi.org/10.21105/joss.00821, 2018.
616 Shankar D, Gopalakrishna VV, Shenoi SSC, Durand F, Shetye SR, Rajan CK, Johnson Z, Araligidad N, Michael G. S.:
617 Observational evidence for westward propagation of temperature inversions in the southeastern Arabian Sea. Geophys Res
618 Lett, 31, 2004. doi:10.1029-2004GL019652
619 Shankar, D., Remya, R., Vinayachandran, P., Chatterjee, A., and Behera, A.: Inhibition of mixed-layer deepening during winter
620 in the northeastern Arabian Sea by theWest India Coastal Current, Climate Dynamics, 47(3-4), 1049–1072, 2016.
621 Shankar, D., Remya, R., Anil, A. C., and Vijith, V.: Role of physical processes in determining the nature of fisheries in the
622 eastern Arabian Sea, 172 (12), 10.1016/j.pocean.2018.11.006, 2018.
623 Shenoi, S. S. C., Shankar, D. and Shetye, S. R.: On the sea surface temperature high in the Lakshadweep Sea before the onset
624 of southwest monsoon, J. Geophys. Res., 104(C7), 15703 – 15712, 1999.
625 Sindhu, B., Suresh, I., Unnikrishnan, A., Bhatkar, N., Neetu, S., and Michael, G.: Improved bathymetric datasets for the
626 shallow water regions in the Indian Ocean, Journal of Earth System Science, 116(3), 261–274, 2007.
627 Swapna, P., Krishnan, R. and Wallace, J.M.: Indian Ocean and monsoon coupled interactions in a warming environment. Clim
628 Dyn, 42**,** 2439–2454, https://doi.org/10.1007/s00382-013-1787-8, 2014.
629 Trainer, V. L., Kudela, R. M., Hunter, M. V., Adams, N. G., and McCabe, R. M.: Climate Extreme Seeds a New Domoic Acid
630 Hotspot on the US West Coast, Front. Clim., 2:571836, doi: 10.3389/fclim.2020.571836, 2020.
631 Thomsen, M. S., Mondardini, L., Alestra, T., Gerrity, S., Tait, L., South, P. M., Lilley, S. A., Schiel, D. R.: Local extinction
632 of bull kelp (*Durvillaea* spp.) due to a marine heatwave, Front. Mar. Sci. 6, 84, https://doi.org/10.3389/fmars.2019.00084,
633 2019.
634 Vijith, V., Vinayachandran, P., Thushara, V., Amol, P., Shankar, D., and Anil, A.: Consequences of inhibition of mixed-layer
635 deepening by the West India Coastal Current for winter phytoplankton bloom in the northeastern Arabian Sea, Journal of
636 Geophysical Research: Oceans, 121, 6583–6603, https://doi.org/10.1002/2016JC012004, 2016.
637 Vinayachandran, P. N., and Shetye, S. R.: The warm pool in the Indian Ocean, Proc. Indian Acad. Sci. (Earth Planet. Sci.),
638 100(2), 165 – 175., 1991.

Vinayachandran, P. N., D. Shankar, J. Kurian, F. Durand, and S. S. C. Shenoi: Arabian Sea Mini Warm Pool and the Monsoon Onset Vortex. Current Science 93, no. 2 (2007): 203–14. http://www.jstor.org/stable/24099306.

Vinayachandran, P.N.M., Masumoto, Y., Roberts, M.J., Huggett, J.A., Halo, I., Chatterjee, A., Amol, P., Gupta, G.V., Singh, A., Mukherjee, A., Prakash, S., Beckley, L. E., Raes, E. J. and Hood, R.: Reviews and syntheses: Physical and biogeochemical processes associated with upwelling in the Indian Ocean. Biogeosciences, 18(22), pp.5967-6029, 2021.

Vörösmarty, C., Fekete, B., and Tucker, B.: River discharge database, Version 1.0 (RivDIS v1. 0), Volumes 0 through 6. A contribution to IHP-V Theme: 1. Technical documents in hydrology series. Paris: UNESCO, 1996.

Wernberg, T., Bennett, S., Babcock, R. C., De Bettignies, T., Cure, K., et al.: Climate- driven regime shift of a temperate marine ecosystem, Science, 353, 169–172, 2016.

Xie, S. P., Hu, K., Hafner, J., Tokinaga, H., Du, Y., Huang, G., and Sampe, T.: Indian Ocean capacitor effect on Indo-Western Pacific climate during the summer following El Nino. J. Clim. 22, 730-747, 2009.

Xie, T., Li, J., Chen, Chen, K., Zhang, Y., Sun, C.: Origin of Indian Ocean multidecadal climate variability: role of the North Atlantic Oscillation. Clim Dyn, 56**,** 3277–3294, https://doi.org/10.1007/s00382-021-05643-w, 2021.

Figure 1: Trend for the MHW days (days/year; left panels), MHW frequency (events/year; middle panels) and MHW intensity (°C/year; right panels) for the annual (a,b,c), pre-monsoon (d,e,f) and summer monsoon (g,h,i) periods. The trends within the 99% confidence limit are marked by stippling. The black boxes represent the north Arabian Sea (NAS) and the southeastern Arabian Sea (SEAS). The trends are calculated for the period 1982-2019.

Figure 2: Boxplots representing the percentage of days experienced heatwaves during (a,d) annual, (b,e) pre-monsoon and (c,f) summer monsoon for the northern Arabian Sea (NAS) and the southeastern Arabian Sea (SEAS). The background shading represents the Niño3.4 index.

Figure 3: Maximum number of heatwave events observed each year across the northern Arabian Sea (top) and the southeastern Arabian Sea (SEAS).

Figure 4: Trends of SST (°C/37 years) over 1982-2019 for (a) annual, (b) pre-monsoon and (c) summer monsoon period. Stippling show regions where the trend is 99% significant based on two-tailed t-test.

Figure 5: Same as Figure 2, but using the detrended SST.

Figure 6: Ratio of MHW days derived using SST and detrended SST based on Equation (3).

Figure 7: (a) Correlation between MHW days based on detrended SST (°C) and major climate modes. Stippling represents regions where correlation is 99% significant. (b) Percentage of co-existing days between observed heatwaves and climate modes for annual, pre-monsoon and summer monsoon periods.

Figure 8: Evolution of observed SST (shading) with model simulated SST overlayed (contour) during April-June 2010. Regions experiencing MHWs are marked by stippling. The blue dot at the northcentral Arabian Sea (63°E/19°N) shows the location where the heat budget analysis was performed.

Figure 9: Same as Figure 8, but plotted daily to show the decaying phase of the heatwave event. The coloured curve on the panel for 2nd June 2010 represents track (and wind speed) of the tropical cyclone *Phet*.

Figure 10: Event line plot of the 2010 pre-monsoon heatwave event at the northcentral Arabian Sea (63°E/19°N). The red shading marks the departure of observed SST from the threshold i.e., the heatwave event. The blue line is the model simulated SST. The green dashed line marks the initiation date of the tropical cyclone *Phet*.

Figure 11: Mixed layer heat budget analysis at the northcentral Arabian Sea (63°E/19°N). The "sum of terms" represents the sum of all terms on the right side of Equation (1).

Figure 12: Model simulated mixed layer depth (top) and anomaly (bottom) for March-June 2010.

Figure 13: Surface heat fluxes, wind speed and mixed layer depth at the northcentral Arabian Sea during March-June 2010.

Figure 14: Cyclone tracks and their wind speeds during 2000-2010 (left) and 2011-2022. The cyclone Nisagra is marked by its propagation dates.

Figure 15: Event line during March-July 2020 at a location off the west coast of India (off Goa). The green dashed line represents the date when the Nisagra cyclone passed over off Goa, India.

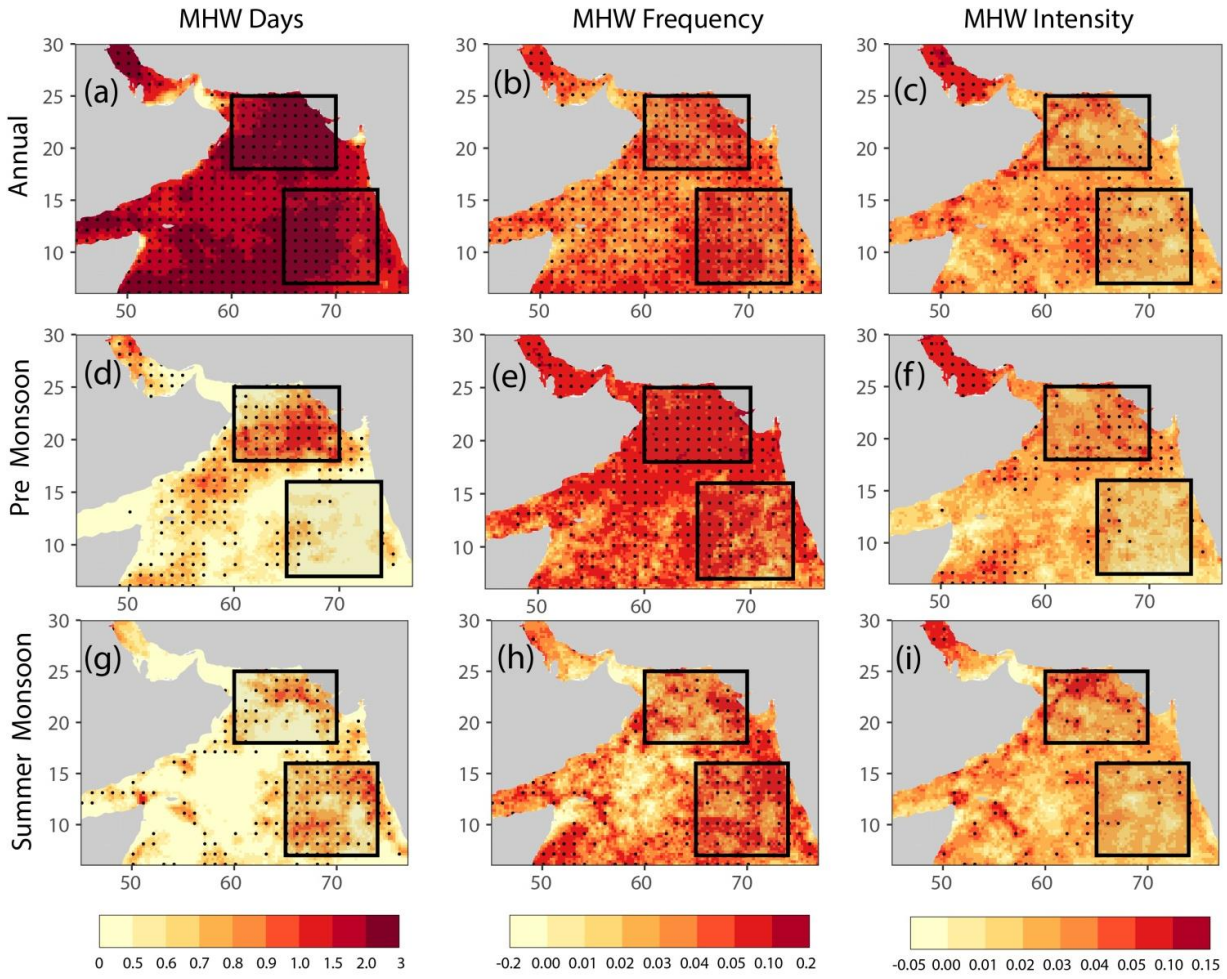

Figure 1: Trend for the MHW days (days/year; left panels), MHW frequency (events/year; middle panels) and MHW intensity (ºC/year; right panels) for the annual (a,b,c), pre-monsoon (d,e,f) and summer monsoon (g,h,i) periods. The trends within the 99% confidence limit are marked by stippling. The black boxes represent the north Arabian Sea (NAS) and the southeastern Arabian Sea (SEAS). The trends are calculated for the period 1982-2019.

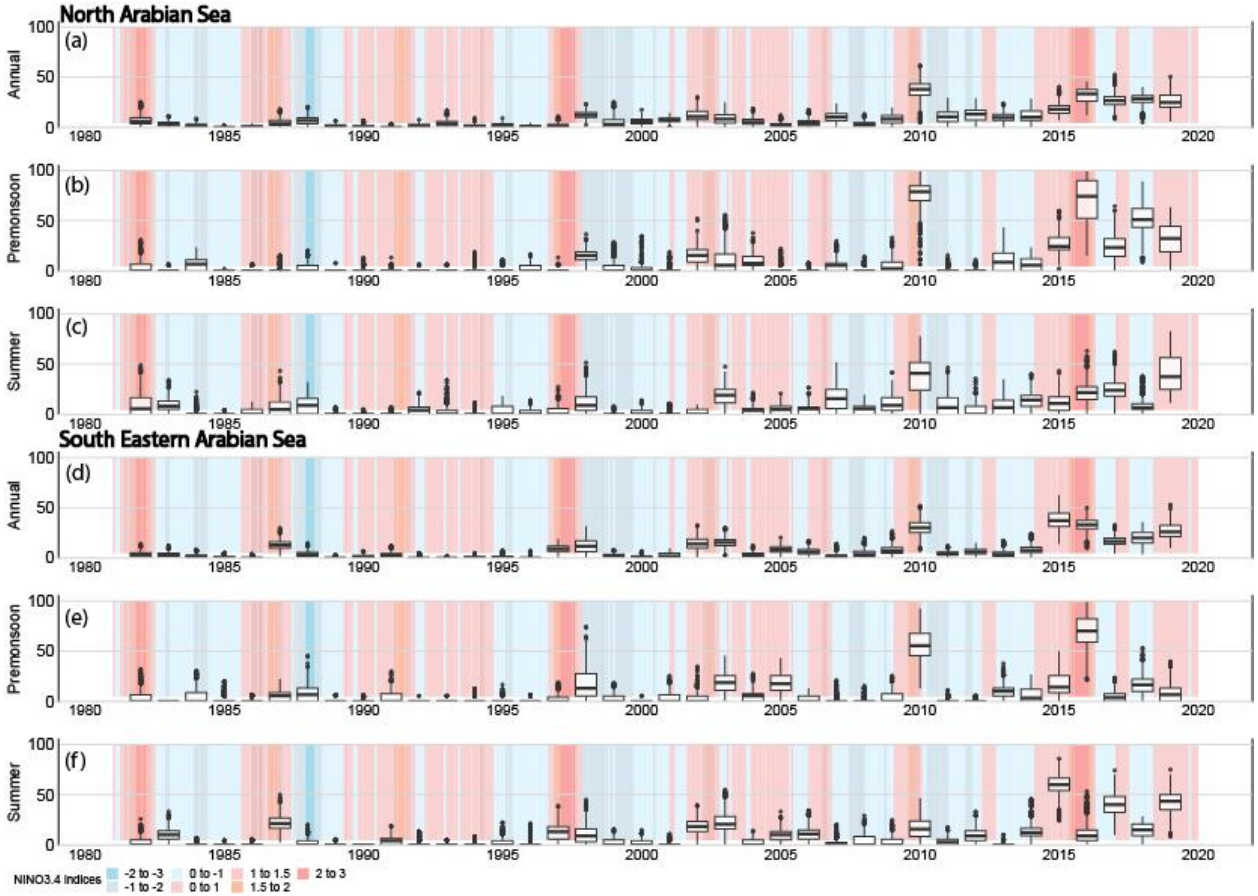

Figure 2: Boxplots representing the percentage of days experienced heatwaves during (a,d) annual, (b,e) pre-monsoon and (c,f) summer monsoon for the northern Arabian Sea (NAS) and the southeastern Arabian Sea (SEAS). The background shading represents the Niño3.4 index.

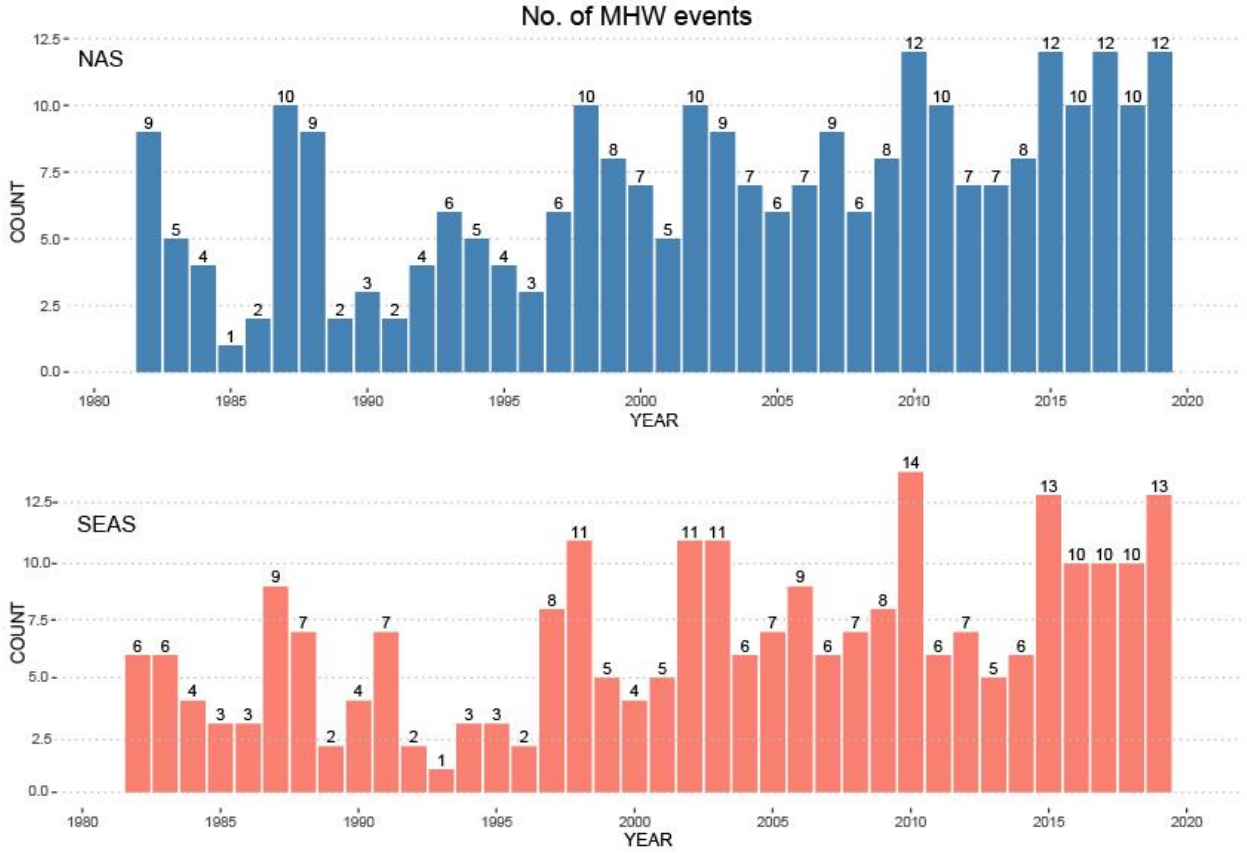

Figure 3: Maximum number of heatwave events observed each year across the northern Arabian Sea (top) and the southeastern Arabian Sea (SEAS).

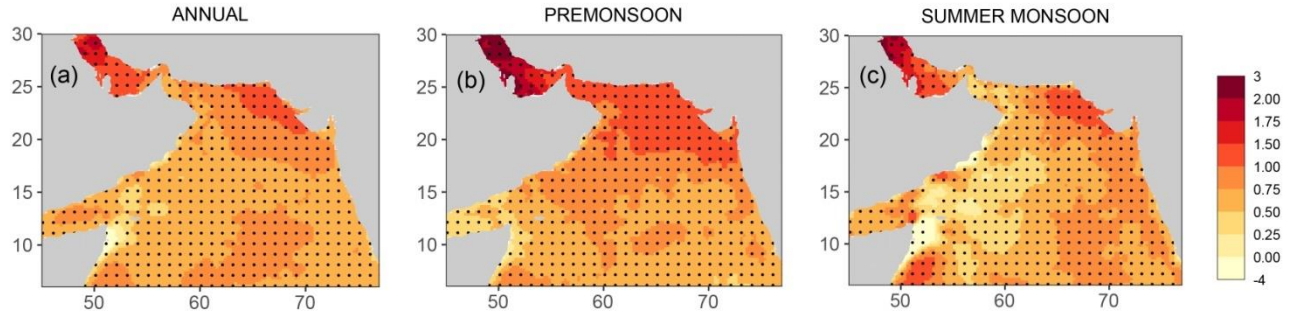

Figure 4: Trends of SST (ºC/37 years) over 1982-2019 for (a) annual, (b) pre-monsoon and (c) summer monsoon period. Stippling show regions where the trend is 99% significant based on two-tailed t-test.

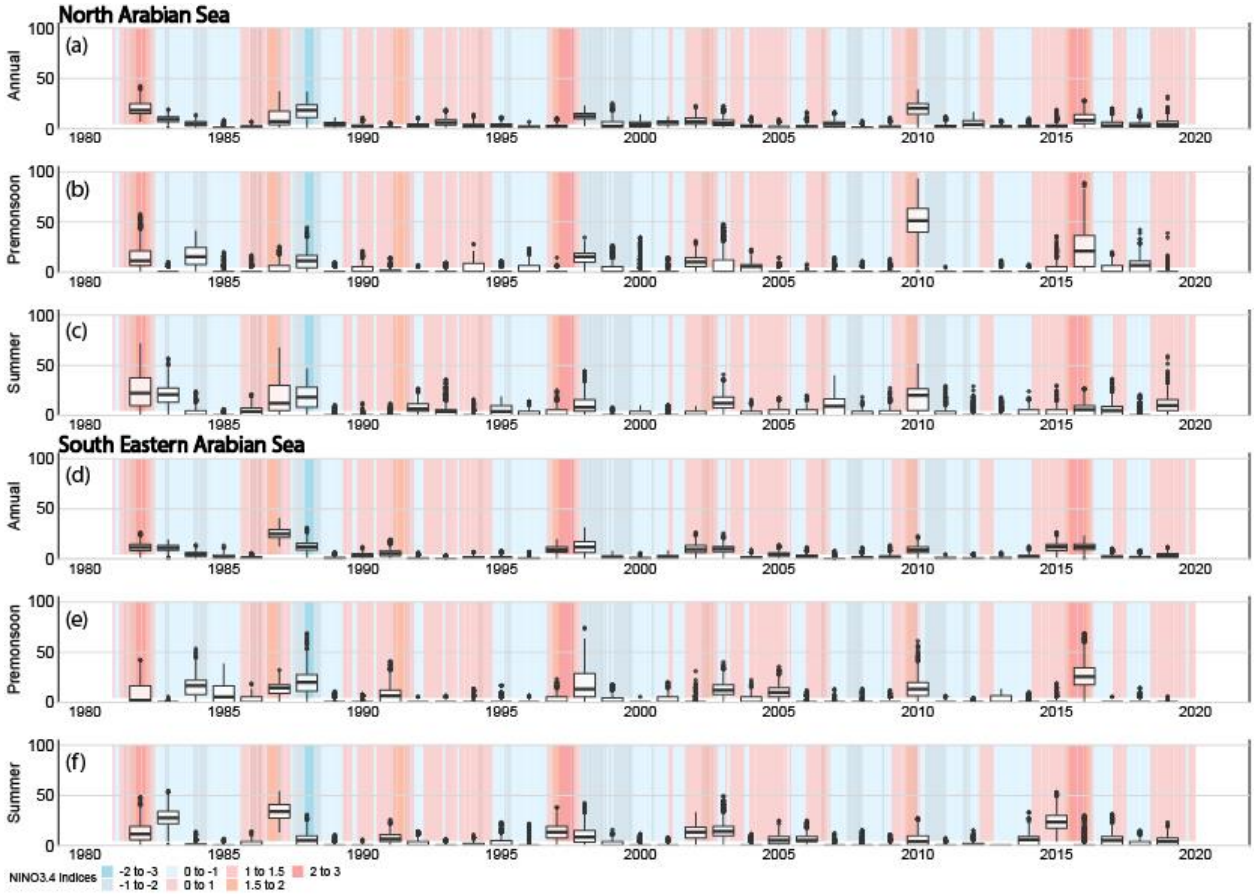

Figure 5: Same as Figure 2, but using the detrended SST.

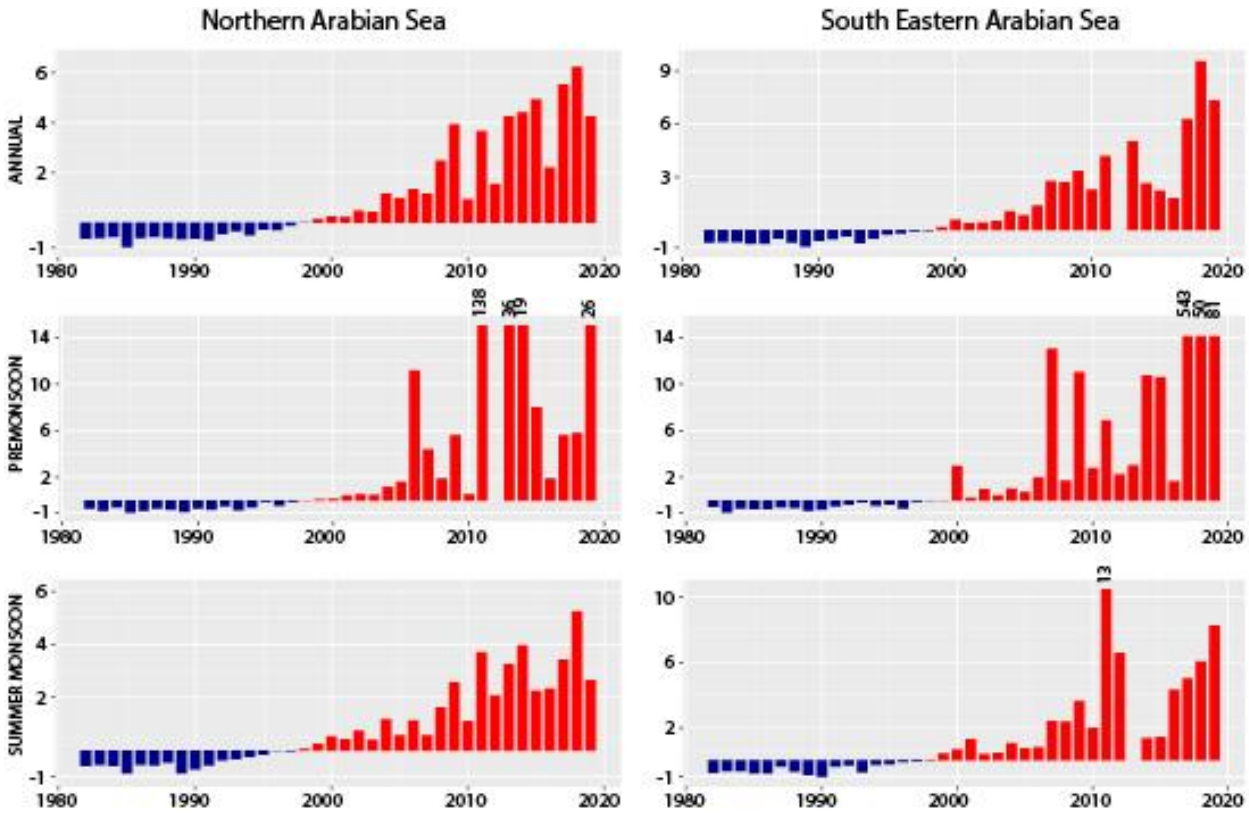

Figure 6: Ratio of MHW days derived using SST and detrended SST based on Equation (3).

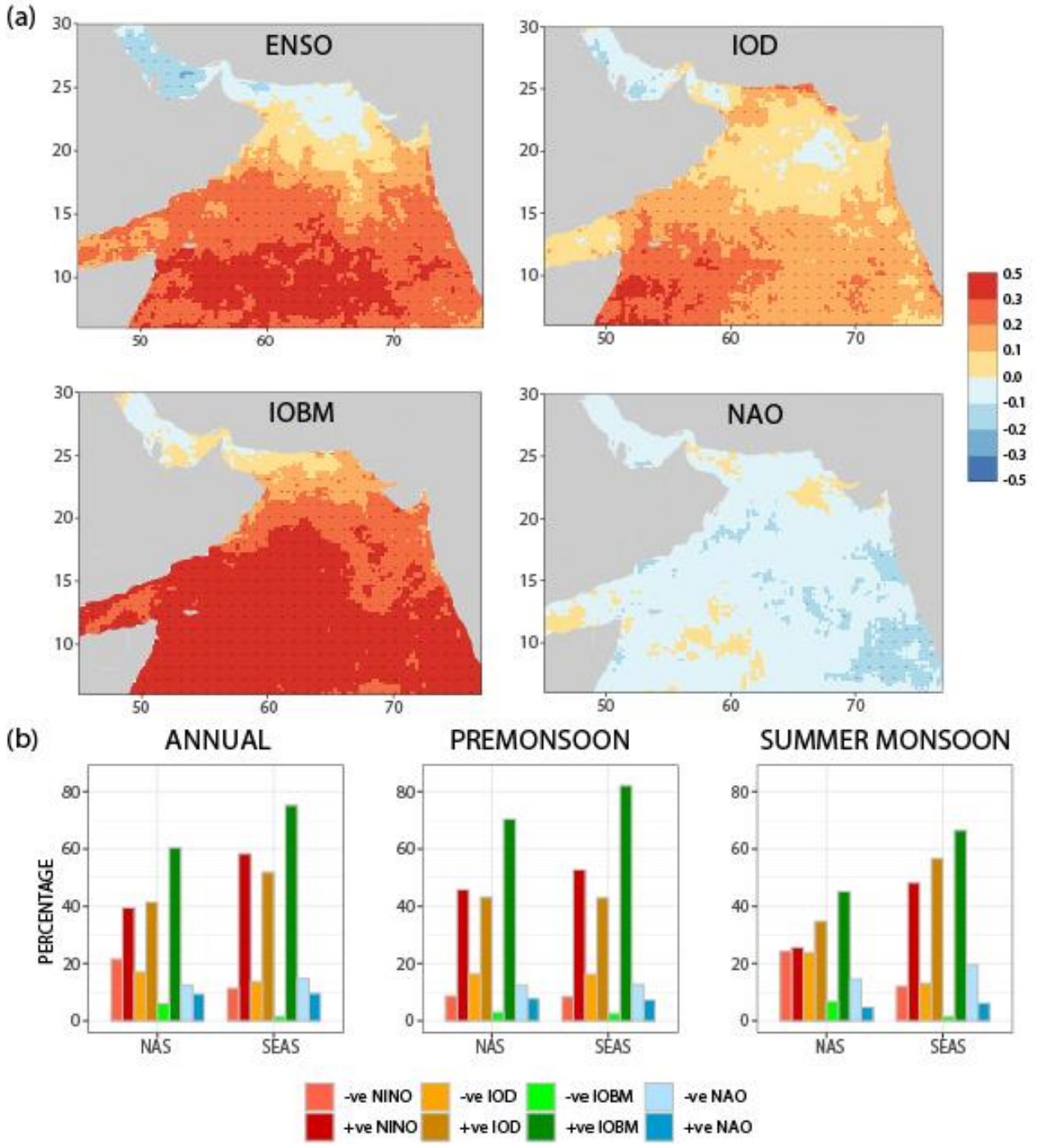

Figure 7: (a) Correlation between MHW days based on detrended SST (°C) and major climate modes. Stippling represents regions where correlation is 99% significant. (b) Percentage of co-existing days between observed heatwaves and climate modes for annual, pre-monsoon and summer monsoon periods.

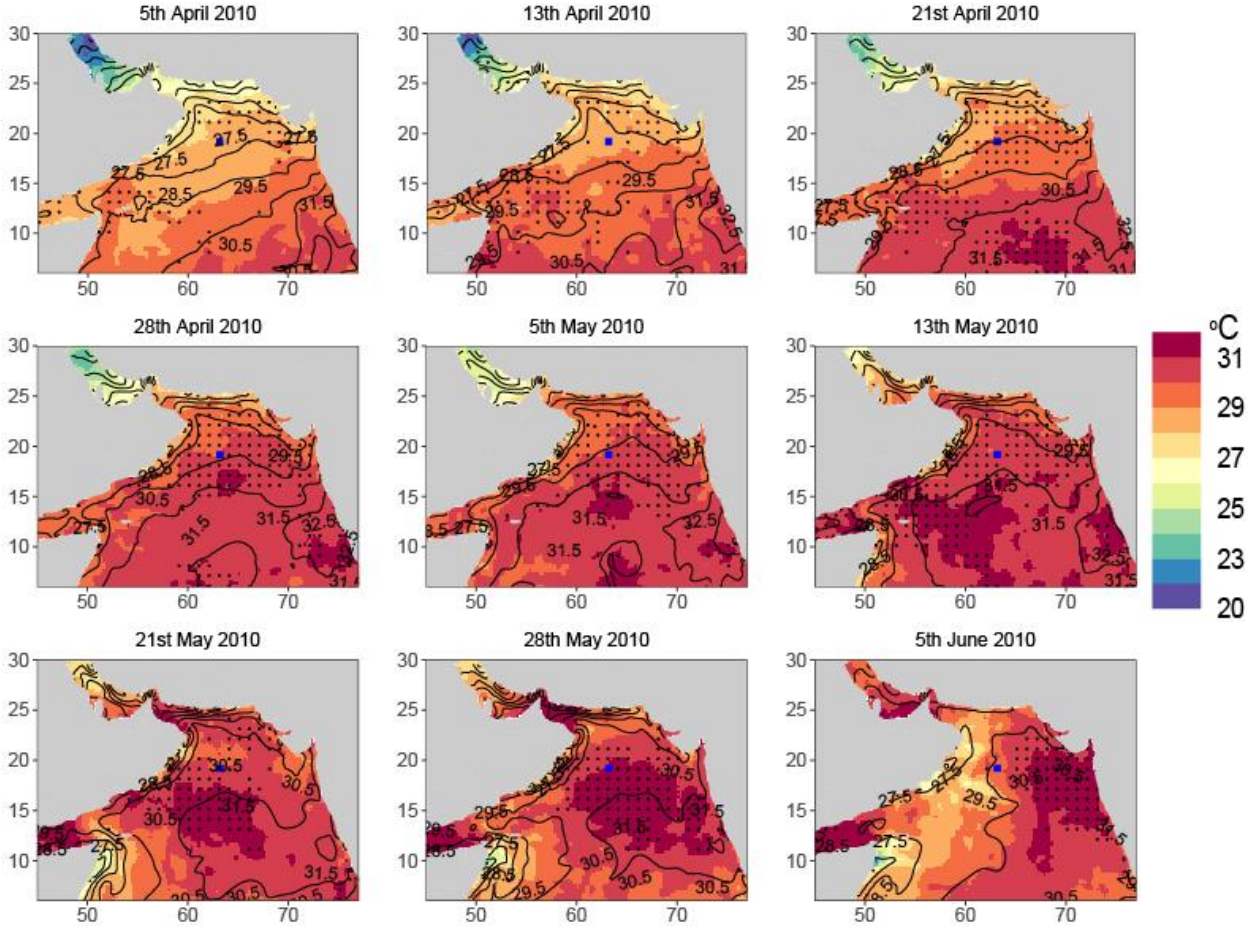

Figure 8: Evolution of observed SST (shading) with model simulated SST overlayed (contour) during April-June 2010. Regions experiencing MHWs are marked by stippling. The blue dot at the northcentral Arabian Sea (63°E/19°N) shows the location where the heat budget analysis was performed.

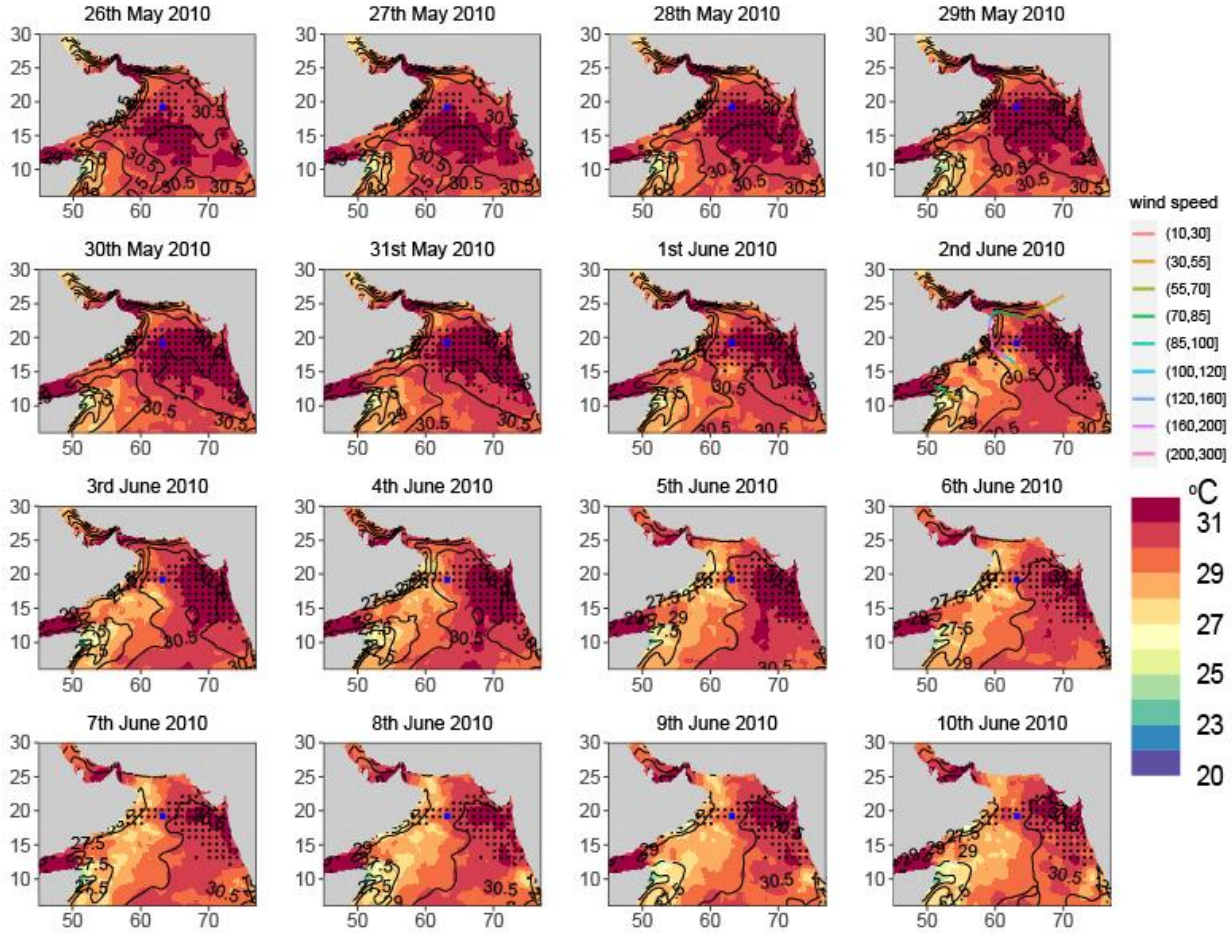

Figure 9: Same as Figure 8, but plotted daily to show the decaying phase of the heatwave event. The coloured curve on the panel for 2nd June 2010 represents track (and wind speed) of the tropical cyclone *Phet*.

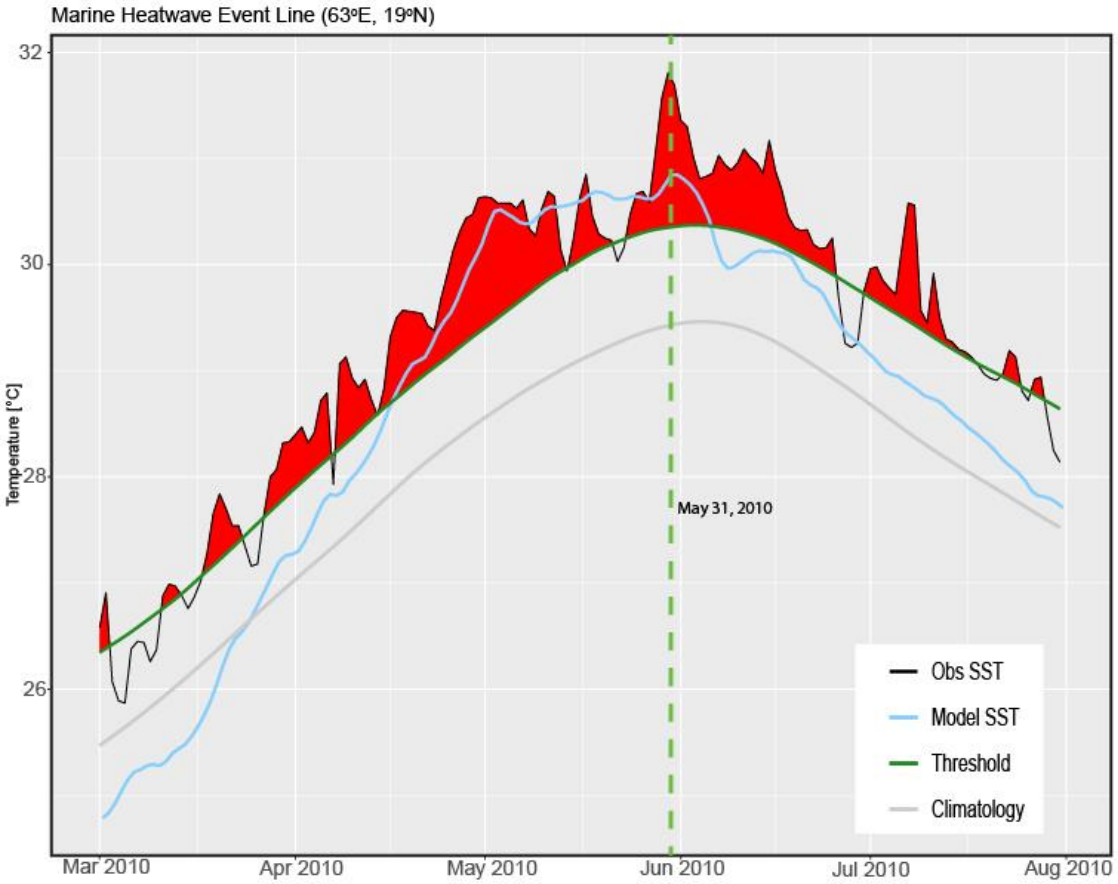

Figure 10: Event line plot of the 2010 pre-monsoon heatwave event at the northcentral Arabian Sea (63ºE/19ºN). The red shading marks the departure of observed SST from the threshold i.e., the heatwave event. The blue line is the model simulated SST. The green dashed line marks the initiation date of the tropical cyclone *Phet*.

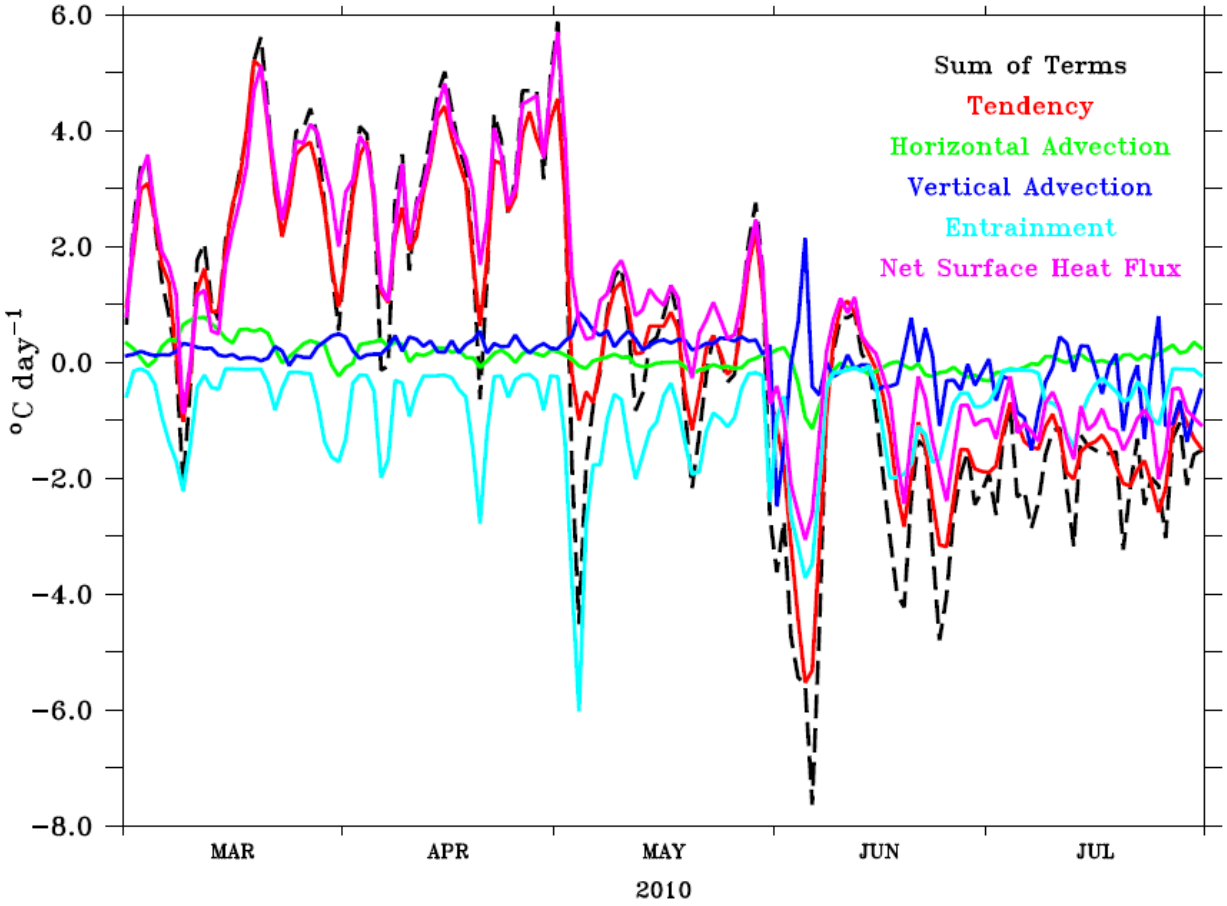

741
742 **Figure 11:** Mixed layer heat budget analysis at the northcentral Arabian Sea (63°E/19°N). The "sum of terms" represents the
743 sum of all terms on the right side of Equation (1).

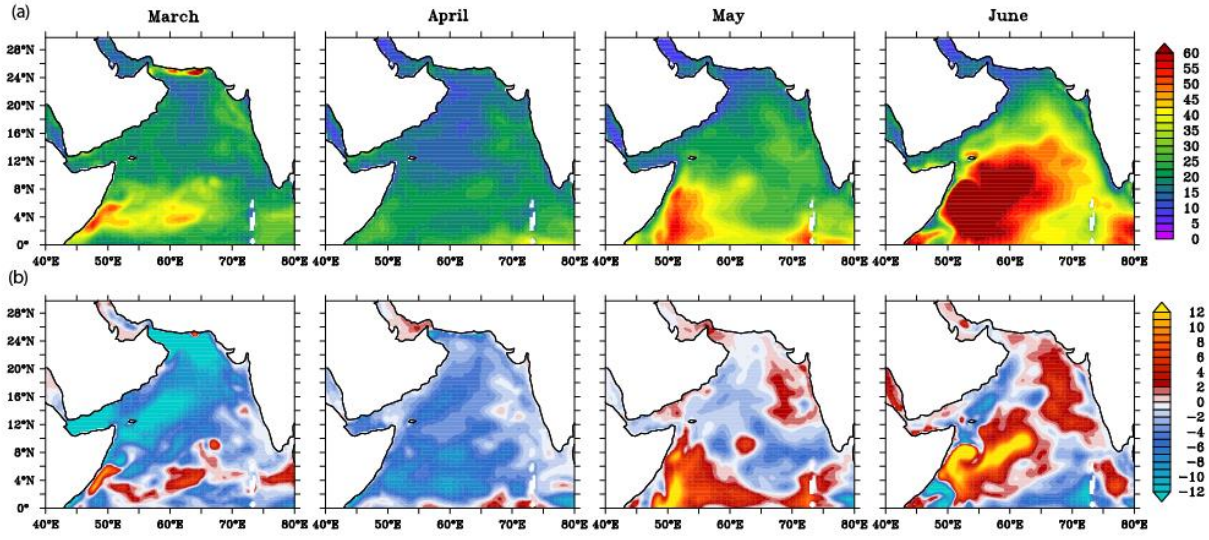

744

745 **Figure 12:** Model simulated mixed layer depth (top) and anomaly (bottom) for March-June 2010.

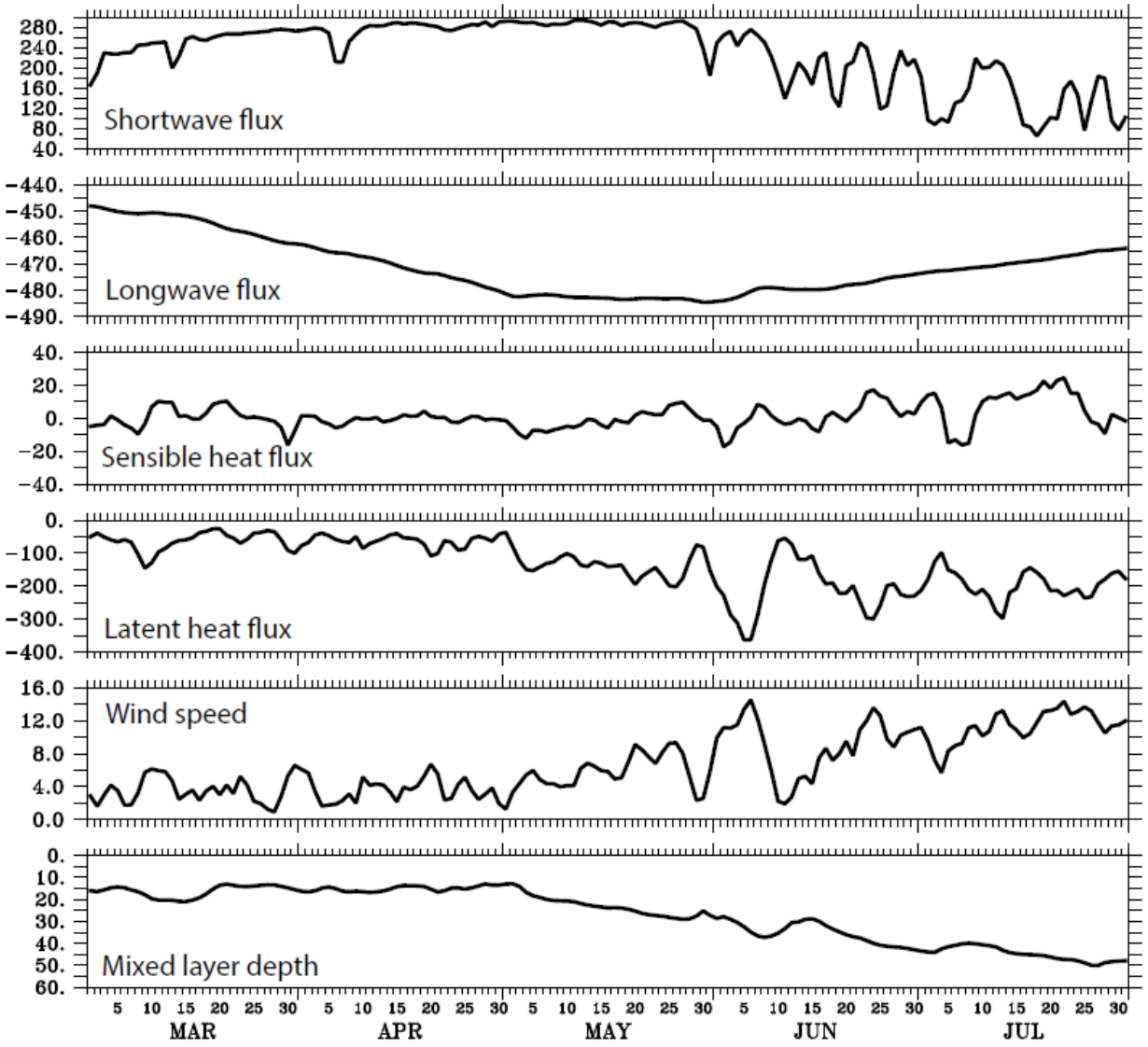

746
747 **Figure 13:** Surface heat fluxes, wind speed and mixed layer depth at the northcentral Arabian Sea during March-June 2010.
748

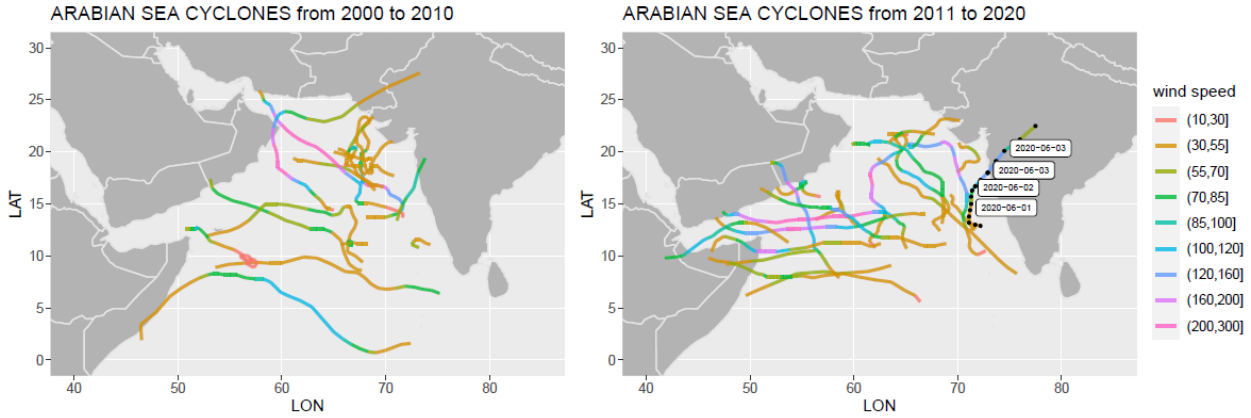

Figure 14: Cyclone tracks and their wind speeds during 2000-2010 (left) and 2011-2022. The cyclone track of Nisagra is marked by its propagation dates.

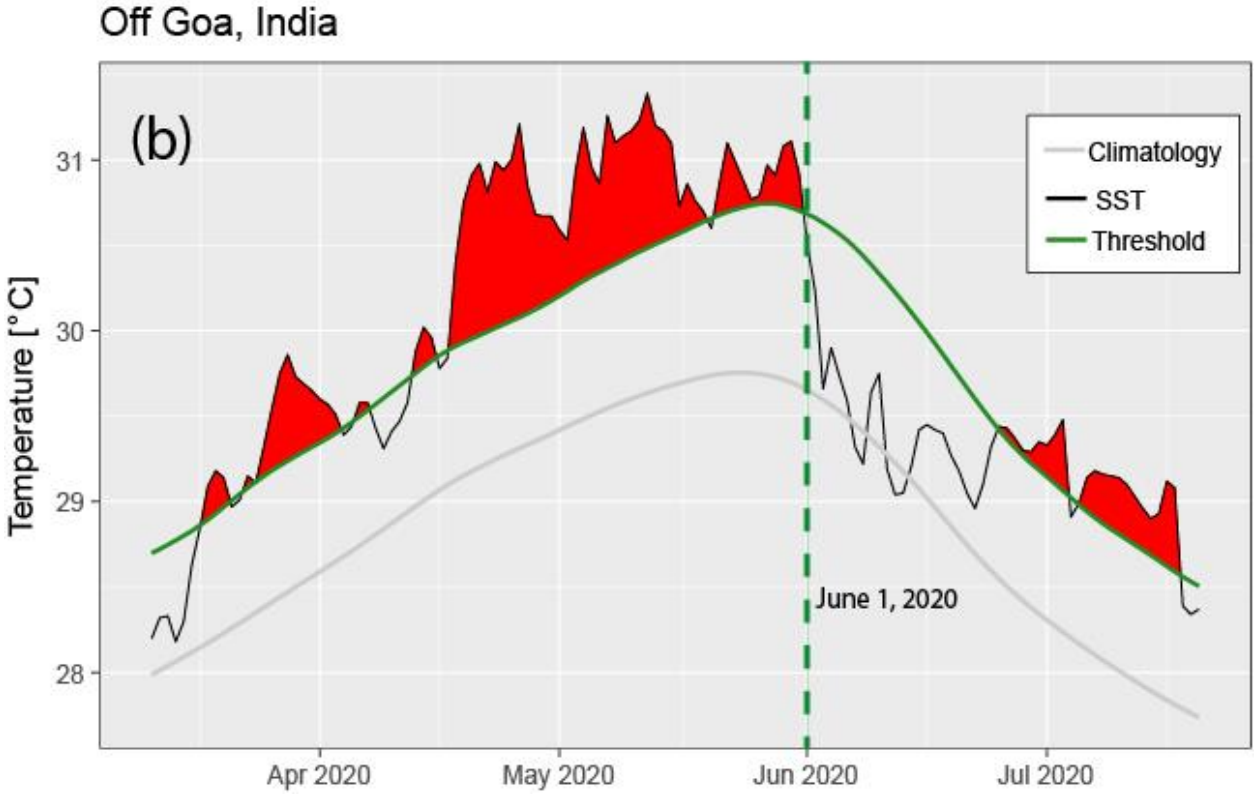

Figure 15: Event line during March-July 2020 at a location off the west coast of India (off Goa). The green dashed line represents the date when the Nisagra cyclone passed over off Goa, India.